UNIVERSITAT POLITÈCNICA DE CATALUNYA
BARCELONATECH
Escola Superior d'Agricultura de Barcelona

Degradation of organic pollutants by metallic particles

Bachelor's thesis

Degree in Biosystems Engineering

Author: Laura Rosell Illa

Supervised by: Eloi Pineda and Josep Sabaté

10/ June/ 2014

Resum

En els últims anys les nanopartícules estan sent àmpliament estudiades per diverses aplicacions tecnològiques en àmbits tan diferents com la medicina, l'electrònica, el medi ambient, la indústria farmacèutica, la cosmètica, la indústria tèxtil i l'agricultura. El principal interès que tenen les nanopartícules radica en la seva gran superfície de reacció, per la qual cosa amb petites quantitats es poden tenir bons resultats. En l'àmbit del medi ambient són molt estudiats el ferro zero-valent cristal·lí i els compostos amorfs a base de magnesi o algun altre component com el zinc que redueixi la seva oxidació.

En aquest projecte l'objectiu principal era avaluar la capacitat de micro-partícules d'un compost amorf de $Mg_{70}Zn_{30}$ en comparació amb micro-partícules metàl·liques de ferro per decolorar un colorant amb estructura azo (N=N). Durant aquest estudi s'ha trobat la metodologia de treball més adequada amb el material disponible als laboratoris de la universitat i s'ha fet una avaluació inicial de la capacitat dels compostos metàl·lics com inductors de la decoloració.

Els resultats obtinguts permeten concloure que la capacitat de decoloració del ferro zero valent és millor que la de l'aliatge semi-amorf de $Mg_{70}Zn_{30}$ en el cas de colorant Reactive Black 5. Tot i això, els resultats no són lo suficientment bons com perquè aquesta tecnologia fos aplicable en el tractament d'aigües residuals tèxtils on els efluents tenen un pH al voltant de la neutralitat i temperatures al voltant de 25 ^{o}C. L'estudi, tanmateix, ha permès optimitzar la metodologia experimental i obre la possibilitat a la realització de proves utilitzant altres compostos metàl·lics a la recerca d'una major capacitat de decoloració.

Resumen

En los últimos años las nanopartículas están siendo ampliamente estudiadas para varias aplicaciones tecnológicas en ámbitos tan diferentes como la medicina, la electrónica, el medio ambiente, la industria farmacéutica, la cosmética, la industria textil y la agricultura. El principal interés que tienen las nanopartículas radica en su gran superficie de reacción, por lo que con pequeñas cantidades se pueden obtener buenos resultados. En el ámbito del medio ambiente son muy estudiados el hierro cero-valente cristalino y los compuestos amorfos a base de magnesio o algún otro componente como el zinc que reduzca su oxidación.

En este proyecto el objetivo principal era evaluar la capacidad de micro-partículas de un compuesto amorfo de $\mathbf{Mg_{70}Zn_{30}}$ en comparación con micro-partículas metálicas de hierro para decolorar un colorante con estructura azo (N = N). Durante este estudio se ha encontrado la metodología de trabajo más adecuada con el material disponible en los laboratorios de la universidad y se ha hecho una evaluación inicial de la capacidad de los compuestos metálicos como inductores de la decoloración.

Los resultados obtenidos permiten concluir que la capacidad de decoloración del hierro cero valiente es mejor que la de la aleación semi-amorfo de $\mathbf{Mg_{70}Zn_{30}}$ en el caso de colorante Reactive Black 5. Sin embargo, los resultados no son lo suficientemente buenos como para que esta tecnología fuese aplicable en el tratamiento de aguas residuales textiles donde los efluentes tienen un pH alrededor de la neutralidad y temperaturas alrededor de 25 ^{o} C. El estudio, por otro lado, ha permitido optimizar la metodología experimental y abre la posibilidad a la realización de pruebas utilizando otros compuestos metálicos en busca de una mayor capacidad de decoloración

Abstract

Nowadays, nanoparticles are studied for many technological applications in various fields, such as medicine, electronics, environmental care, pharmaceuticals, cosmetics, textiles and agriculture. The main interest of nanoparticles is their high surface reactivity; small amount of material has a large reactive surface area and, therefore, provides good results. In remediation zero-valent iron and amorphous magnesium-based alloys, with zinc addition to reduce the oxidation, have been studied.

The objective of this work is to evaluate the application of $Mg_{70}Zn_{30}$ metallic glass powders in to the degradation process of azo dyes (N=N) and compare these results with Fe metallic powders. During this study, the most suitable working method with the equipment available in the laboratories of university has been found. An initial assessment of the ability of the metal compounds as inducers of decolourization was performed.

Eventually, the results obtained indicate that the capacity of zero-valent iron is better than that of the semi-amorphous alloy $Mg_{70}Zn_{30}$ in the case of decolourization of Reactive Black 5 dye. However, the results are not good enough for their application in the treatment of textile wastewater effluents which have a pH around neutrality and temperatures around of 25ºC. However, this study has permitted to optimize the experimental method and it opens the possibility to test the decolourization of other metal compounds.

TABLE OF CONTENTS

List of figures

Chapter 1: Introduction

Chapter 3: Materials and Methods

Chapter 4: Results

List of tables

Chapter 1: Introduction

Chapter 3: Material and Methods

Chapter 4:Results

Acknowledgements

I would like to thank my supervisors for their help; Eloi Pineda and Josep Sabaté. And the laboratory technicians, specially Maria Rodríguez. Also the PhD students Chaoren Liu and Fuqiang Zhai for their help and patience during synthesis and analysis of particles. All the CRnE personnel , particularly Trifon Trifonov and Joan Aymami. In addition, I would like to thank the research group of materials and thermodynamics of the Physics Department at UdG(Universitat de Girona), in particular Professor Joan Josep Suñol who provided many useful information, materials and equipment. Finally, I would like to thank my classmates, friends and family for all the moments that we shared and their emotional support.

1. Introduction

1.1. Actual context

Before the mid of the nineteenth century only natural dyes were used. Nowadays, however, synthetic organic compounds are the most part of the dyes used in textile industry. Synthetic dyes are more easy to use, they show higher color intensity and have better thermal behavior for a lower cost than natural dyes[1].

In the last years the industrial processes have been optimized and the internal emissions have been reduced. For example, in order to neutralize the effluent acetic acid was substituted by formic acid, which the increase in COD(Chemical Oxygen Demand) is not so high[2]. However, the textile industrial pollution is still a major trouble[3], as it showed in Table 1.1. The wastewater from textile plants is classified as the most polluting of all industrial sectors[4]. The main environmental consequence is the presence of color, decreasing the transparency and the amount of dissolved oxygen and, consequently, causing a harmful effect on the photosynthetic activity of plants and algae [1].

The characteristics of textile effluents had a high differences in COD, BOD (Biochemical Oxygen Demand), colour, C (carbon), N(nitrogen), P(phosphorous), salts or SS (Suspended Solids) depending on the different industrial process stages and the kind of fiber to tint[4] . Some of these characteristics are detailed in Table 1.1.

Table1 .1 Characteristics of pollution load of textile effluents depending on the kind of fiber. [2]

Pollution load of textile effluents

Parameter	Flock	Thread	Cotton fabric	Wool fabric	Knitting fabric	Tooling	Wool wash
pH	7-12	7-11	8-13	5.5-8	5.5-9	7-10	8-11
COD(mgO_2/L)	3000-7000	500-1000	1500-3000	300-1500	800-1800	2000-4000	20000-60000
BOD(mgO_2/L)	1000-2200	200-350	400-1000	100-600	250-500	500-1500	6000-20000
SS(mg/l)	100-300	50-150	100-300	100-200	100-200	200-600	6000-20000
Colour Pt-Co/l	400-4000	400-1000	400-3000	200-1500	200-2000	1000-6000	100-200

Chemical oxygen demand (COD) test is used to indirectly measure the amount of organic compounds in water. It measures everything that can be chemically oxidized. It is expressed in milligrams of oxygen per liter (mg O_2/L), which indicates the mass of oxygen consumed per liter of solution. COD is a useful measure of water quality.

Biochemical Oxygen Demand (BOD) is used to measure the amount of oxygen needed by organisms. The BOD value is most commonly expressed in milligrams of oxygen consumed per litre of sample during 5 days of incubation at 20^{o}C.

Suspended solids (SS) include all small solid particles suspended in water as a colloid or due to the motion of the water.

Water is shown colored when visible radiation is absorbed from dissolved materials, or when light is reflected on suspended solids. These two sources of color are the base for the distinction between the pseudo and true color. The pseudo color is due to absorption as well as light reflection. The true color depends exclusively from the kind and quantity of the dissolved substances. The most commonly used units mg Pt-Co / l are defined as color measurement units. Platinum-cobalt color scale is based on stable liquid color standards made from chloroplatinate solutions. The scale ranges from distilled water at 0 to a stock solution of 500 (parts per million of platinum cobalt to water).

The effects of dyes in human health depend on the time of exposition and exposition mode. The majority of dyes when are ingested, they are excreted by the body. Some effects are contact dermatitis or respiratory sensitization[1]. However, some azoic dyes, more or less 3000 dyes used currently in industry, are potentially carcinogenic[5,6]. This toxicity is caused by aromatic amines produced in oxidative processes, hydrolysis or the azo bond reduction[7].

1.2. Azo dyes

One of the most commonly used classifications for dyes are based on the chemical structure. In this classification, dyes are grouped from most to least important: azo, carbonyl, phthalocyanine, arilcarbonyl ion, sulphur, polymethine and nitro[1,8]. Chemical structures are shown in Figure1.1

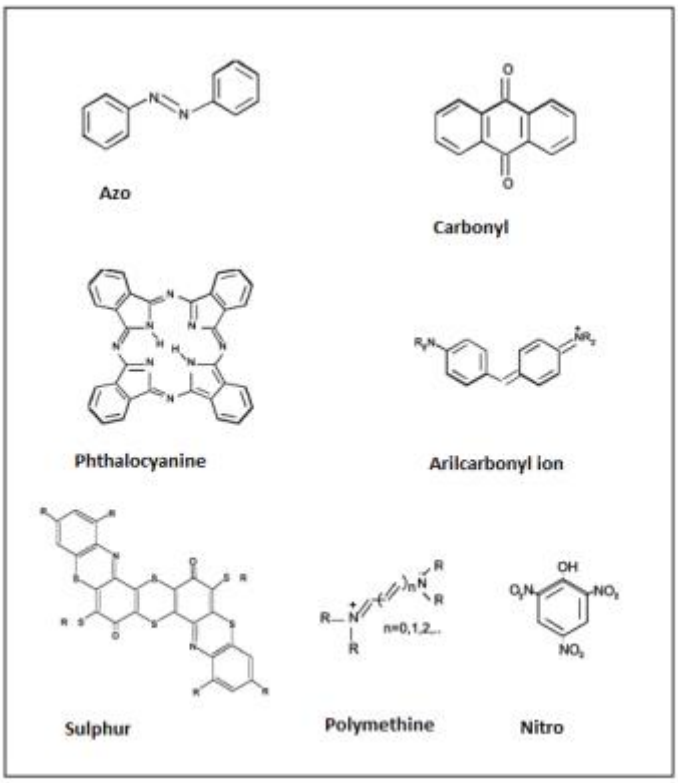

Figure 1.1. Chemical structure of the different kinds of dyes. [1]

Azo colorants are the most important group of synthetic dyes and pigments, representing 60 - 80% of all organic colorants[9]. They are used widely in substrates such as textile cellulose fibers, leather, plastics, papers, hair, mineral oils, waxes, foodstuffs and cosmetics. They are characterized by a functional azo group, that consists in a double bond –N=N-, that normally attaches at two aromatic rings[5]. The properties of this kind of dyes are a wide range of shades and high color intensity, fastness to light and resistance to heat, water and other solvents. They also show a remarkably high industrial performance [1].

In the last years, decontamination of azo dyes using metallic nano or micro-particles, microorganisms and other methods have been studied. The most common azo dyes are Reactive Black 5[7,10–17], Methylene Blue[18], Methyl Orange[19–21], Orange I[21], Orange II[6,21–24], drimarene red, remazol brown, drimarene navy, tartrazine[11], sunset yellow FCF[11], procion Navy H-EXL[7], direct Blue 6[25,26], Sudan I[8], Congo Red[8], Amaranth[8], Acid Orange 7[8].

1.3. Micro-particles

Micro-particles and nanoparticles exist widely in the natural world, for example as the products of photochemical and volcanic activity, and they are created by plants and algae too. Micro-particles

have also been created for thousands of years by human activity as products of combustion and food cooking, and recently from vehicle exhausts.

Micro-particles and nanoparticles are of interest because of the unique properties, that their exhibit compared with larger particles of the same materials such as high specific surface area , with abundant reactive sites on the surface as a consequence of a large fraction of atoms located on the exterior rather than in the bulk[22,27] . Micro-particles have a range of potential applications, for example in new cosmetics, textiles, paints, medicine, environmental remediation, electronics and agriculture[28]. They can also be arranged into layers on surfaces and they are relevant for a wide range of potential applications acting as catalysts. Applications of some nanoparticles are resumed in Figure 1.2.

Source	Type of nanoparticle	Quantity used in terms of tons	Application/uses
Metals and alkaline earth metals	Ag	High	Antimicrobials, paints, coatings, medical use, food packaging
	Fe	High	Water treatment
	Pt group metals	High	Catalysts
	Sn	Unknown	Paints
	Al	High	Metallic coating/plating
	Cu	Unknown	Microelectronics
	Zr	High	
	Se	Low	Nutraceuticals, health supplements
	Ca	Low	Nutraceuticals, health supplements
	Mg	Low	Nutraceuticals, health supplements
Metal oxides	TiO_2	High	Cosmetics, paints, coatings
	ZnO	Low	Cosmetics, paints, coatings
	CeO_2	High	Fuel catalyst
	SiO_2	High	Paints, coatings
	Al_2O_3	Low	Usually substrate bound, paintings
Carbon materials	Carbon black	High	Substrate bound, but released with tyre wear
	Carbon nanotubes	Medium–High	Used in a variety of composite materials
	Fullerenes (C60-C80)	Medium–High	Medical and cosmetics use
Miscellaneous	Nanoclay	High	Plastic packaging
	Ceramic	High	Coatings
	Quantum dots	Low	Different compositions
	Organic nanoparticles	Low	Vitamins, medicines, carriers for medicines and cosmetics, food additives and ingredients

Figure 1.2. Production of nanoparticles from different sources and respective applications. [27]

Nanoparticles and micro-particles, similarly to bulk materials, may be classified according to their atomic-scale structure, this is the regularity in which atoms or ions are arranged. It is important because their properties change depending on the structure.

A crystalline material is one in which the atoms are situated in a periodic or repeating array over large atomic distances. All metals form crystalline structures under normal solidification conditions. When the long-range atomic order is absent, these materials are amorphous or non-crystalline[29].

Nowadays, to remove pollutants from water many kinds of nanoparticles or micro-particles are studied.

Nanoparticles that are activated by light, such as, large band-gap semiconductor TiO_2 and ZnO are studied for their ability to remove organic contaminants from various media[30].

Nanoescale iron particles are effective for the transformation and detoxification of a variety of common environmental contaminants, such as chlorinated organic solvents, organochlorine pesticides, and polychloro biphenyls. In addition metallic zero-valent iron and other materials, for instance metallo-porphyrinogens have been tested for degradation of tetrachlorethylene, trichloroethylene, and carbon tetrachloride under anaerobic conditions. Moreover, nanoparticles such as poly(amido-amine) dendrimers (they are repetitively branched molecules) can serve as chelating agents, an can enhance ultrafiltration of a variety of metal ions (Cu(II), Ag(I), Fe(III), and others) by attaching to functional groups, for example primary amines, carboxylates, and hydroxymates[22]. List of common contaminants that can be transformed by zero-valent Iron are in Figure 1.3.

Chlorinated methanes	Trihalomethanes
Carbon tetrachloride (CCl_4)	Bromoform ($CHBr_3$)
Chloroform ($CHCl_3$)	Dibromochloromethane ($CHBr_2Cl$)
Dichloromethane (CH_2Cl_2)	Dichlorobromomethane ($CHBrCl_2$)
Chloromethane (CH_3Cl)	Chlorinated ethenes
Chlorinated benzenes	Tetrachloroethene (C_2Cl_4)
Hexachlorobenzene (C_6Cl_6)	Trichloroethene (C_2HCl_3)
Pentachlorobenzene (C_6HCl_5)	*cis*-Dichloroethene ($C_2H_2Cl_2$)
Tetrachlorobenzenes ($C_6H_2Cl_4$)	*trans*-Dichloroethene ($C_2H_2Cl_2$)
Trichlorobenzenes ($C_6H_3Cl_3$)	1,1-Dichloroethene ($C_2H_2Cl_2$)
Dichlorobenzenes ($C_6H_4Cl_2$)	Vinyl chloride (C_2H_3Cl)
Chlorobenzene (C_6H_5Cl)	Other polychlorinated hydrocarbons
Pesticides	PCBs
DDT ($C_{14}H_9Cl_5$)	Dioxins
Lindane ($C_6H_6Cl_6$)	Pentachlorophenol (C_6HCl_5O)
Organic dyes	Other organic contaminants
Orange II ($C_{16}H_{11}N_2NaO_4S$)	N-nitrosodimethylamine (NDMA) ($C_4H_{10}N_2O$)
Chrysoidine ($C_{12}H_{13}ClN_4$)	TNT ($C_7H_5N_3O_6$)
Tropaeolin O ($C_{12}H_9N_2NaO_5S$)	Inorganic anions
Acid Orange	Dichromate ($Cr_2O_7^{2-}$)
Acid Red	Arsenic (AsO_4^{3-})
Heavy metal ions	Perchlorate (ClO_4^-)
Mercury (Hg^{2+})	Nitrate (NO_3^-)
Nickel (Ni^{2+})	
Silver (Ag^+)	
Cadmium (Cd^{2+})	

Figure 1.3. Common environmental contaminants that can be transformed by nanoescale iron particles[22].

Metallic or zero-valent iron(Fe^0) has been determined to be an effective material for the removal of a variety of important organic contaminants from water[6,12,21,23,25]. It is a moderate reducing agent. Its standard reduction potential makes Fe^0 a reducing agent for many redox-labile substances, including hydrogen ions, carbonate, sulfate, nitrate, and oxygen. Azo dyes can be reduced by iron, because the reduction of the cromophoric group is thermodynamically favorable[22].

$$Fe^0 \rightarrow Fe^{2+} + 2e^- \qquad E_0 = -0{,}44\ V \qquad (1.1)$$

In addition, magnesium metal (Mg^0) exhibits superior performance and has been used in combination with palladium or calcium , which act as a catalyst for the reaction. For instance, combination of magnesium and palladium gave good and fast results for dechlorination of DDT, pentachlorophenol, and phenol[11]. Amorphous $Mg_{73}Zn_{21,5}Ca_{5,5}$ particles were effective to degrade Direct Blue 6[12,25]. The major advantage of the magnesium-based system are their high negative reduction potential of Mg^{2+}/Mg^0 (-2,2 V) as compared to Fe^{2+}/Fe^0 (0,44 V).

$$Mg^0 \rightarrow Mg^{2+} + 2e^- \qquad E_0 = -2{,}2\ V \qquad (1.2)$$

The reaction of azo dye degradation is initiated by corrosion of zero-valent metals, such as iron or magnesium, as are shown in reactions (1.1) and (2.2). Then, electrons derived from the metal are captured by protons to generate nascent hydrogen, which in the presence of hydrogenating metal catalyst yields metal hydride. The metal hydride reacts via aromatic nucleophilic substitution[31] with target compounds to produce the corresponding reduced products. Another option is that electrons may be donated directly to the functional groups of target compounds[11].

1.4. Treatment plants

This work studies the application of metallic micro-particles as catalysts in wastewater treatment. In order to apply this method it is necessary to know the configuration of the treatment plants that industries use. As it is shown Table 1.1 the characteristics of textile effluents have large differences. As a consequence of this, the configuration of textile wastewater plants may change considerably, as they are shown in Figures 1.4-1.9. Here, I will briefly introduce the main different types of wastewater plants.

Activated sludge plant.

The biological activated sludge process offers a good elimination of COD and BOD. However it has bad color elimination and these plants require experienced staff, who has good control of raw materials in the textile process[2]. The general diagram of this kind of treatment plants are illustrated in Figure1.4.

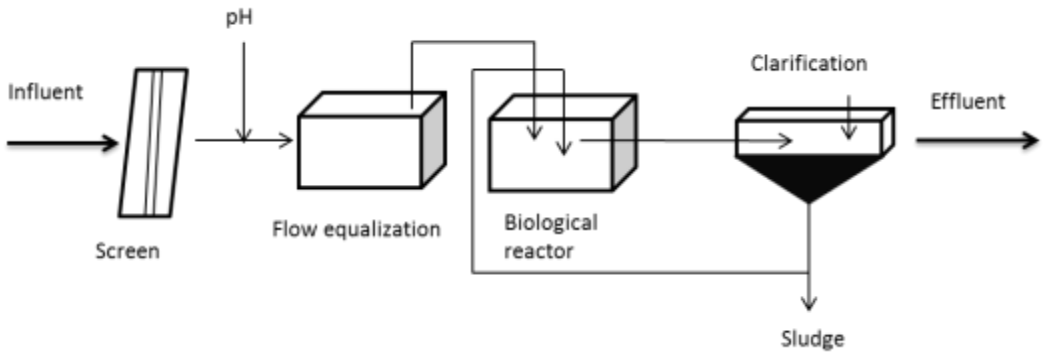

Figure 1.4. Activated Sludge plant.[2]

Screening is the first unit operation encountered in wastewater treatment plants. A screen is a device with openings, which is used to remove objects, such as, plastic, paper, textiles, to prevent damage and clogging of the plant installations[32].

Flow equalization is used to minimize the variability of the flow rates and composition in the subsequent treatment operations and processes[32].

The sedimentation tank is used to remove readily settleable solids and floating material and thus reduce the suspended-solid content. When a liquid containing solids in suspension is placed in a relatively quiescent state, those solids having a higher specific gravity than the liquid will tend to settle, and those with lower specific gravity will tend to rise[32].

The dyes degradation by microorganisms is an inexpensive process. They degrade partially or completely the initial compounds. However, the dye biodegradability depends on chemical structure[1,7].

Biological activated sludge

The biological activated sludge with active carbon or decolorizing polymers process offers a good elimination of COD, BOD and color. Moreover, it produces a good quality effluent. But these plants require experienced staff, with good control of raw materials in the textile process[2]. The general diagram of this kind of treatment plants is illustrated in figure1.5.

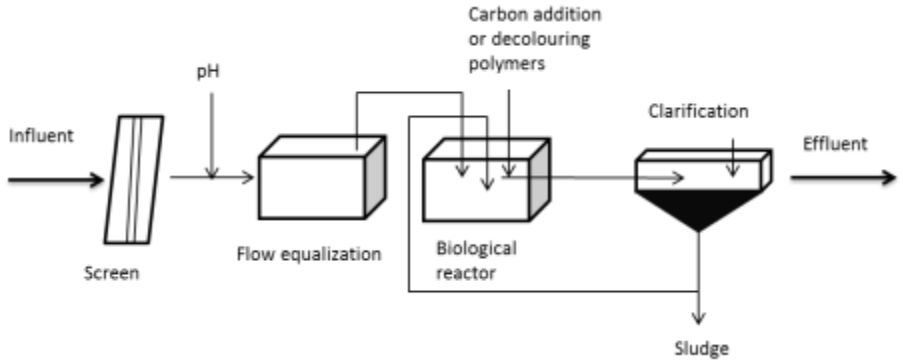

Figure 1.5. Activated sludge plant with active carbon or decolorizing polymers[2].

Chemical coagulation process

The chemical coagulation process treatment offers a good elimination of COD and BOD , color and SS if microorganisms can survive in the flow equalization tank. Nevertheless, large amount of sludge is generated[2]. The general diagram of this kind of treatment plants are illustrated in the figure 1.6.

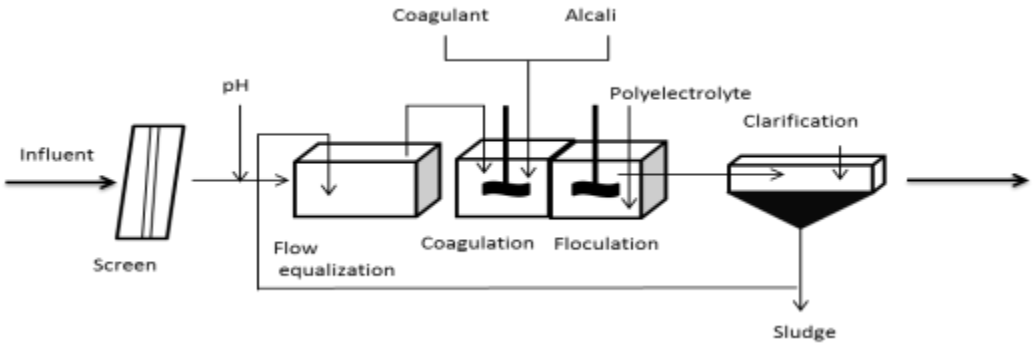

Figure 1.6. Chemical coagulation and flocculation[2].

Coagulation is a process that consists in destabilization of the colloidal suspension by the addition of chemical reagents with opposite charged particles in order to neutralize and reduce the forces that maintain balance in the water. Normally, the reagents are metallic salts of aluminum or iron[1,32]

Flocculation is a process that consists in stabilized colloidal particles contacting with each other and establishing chemical bonds between dye molecules, called floccules. Reagents are anionic or cationic polyelectrolyte and nonionic type, natural or synthetic, depending on the structure of the molecules to eliminate[1,32].

Biological activated sludge with a tertiary process

The biological activated sludge with a tertiary process treatment offers excellent results. But normally the costs are high[2]. The general diagram of this kind of treatment plants is illustrated in figure1.7.

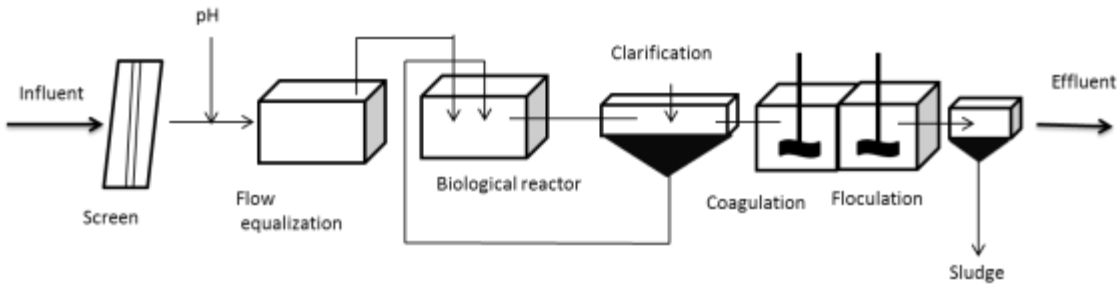

Figure 1.7. Biological activated sludge with a tertiary process treatment[2].

Chemical coagulation process combined with trickling filter

The chemical coagulation process combined with trickling filter process offers good global results, with moderate costs[2]. The general diagram of this kind of treatment plants is illustrated in figure1.8.

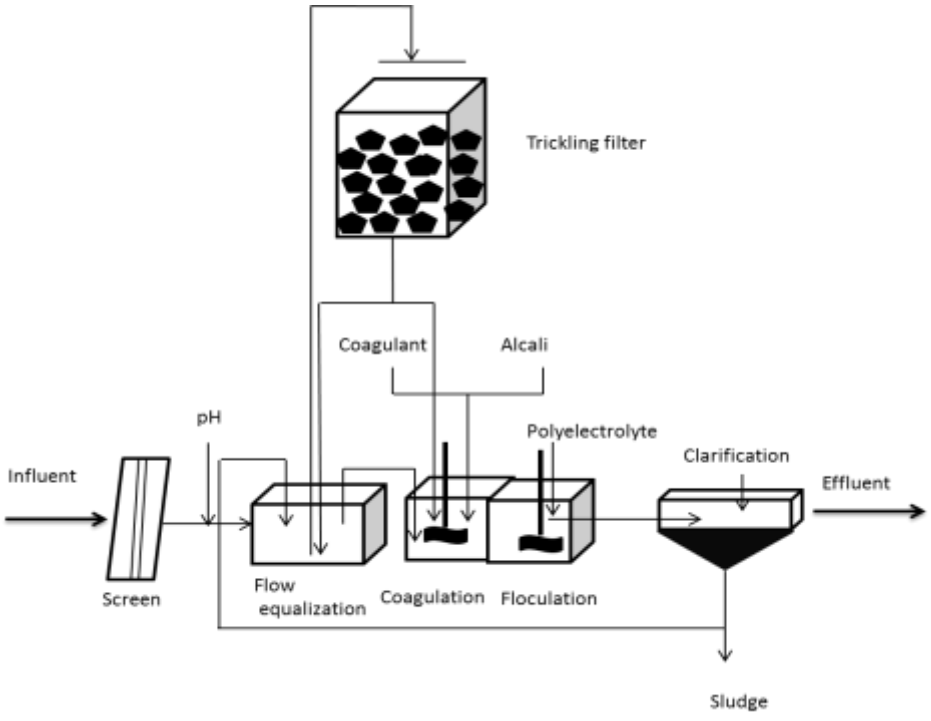

Figure 1.8. Chemical coagulation process combined with trickling filter[2].

The trickling filter consists of a fixed bed of broken stones, plastic media or other types of filling. The contact bed was filled with wastewater from the top, and the wastewater was allowed to

contact the media for a short time. The bed is then drained and allowed to rest before the cycle is repeated. This process causes the growth of a biofilm covering the bed of the media[32].

Wastewater treatment combined with urban water treatment

Wastewater treatment combined with urban water treatment permit to obtain goods results if the volumetric flow rate of urban water is higher than textile water. Otherwise the wastewater treatment plant should be modified in order to remove color. This involving the use of coagulants, decolorizing agents, ozone… [2]

Membrane bioreactor

Membrane bioreactor (MBR) wastewater treatment plant obtains excellent results. It permits the reuse of the effluent, and the costs are moderate[2]. The general diagram of this kind of treatment plants is illustrated in figure1.9.

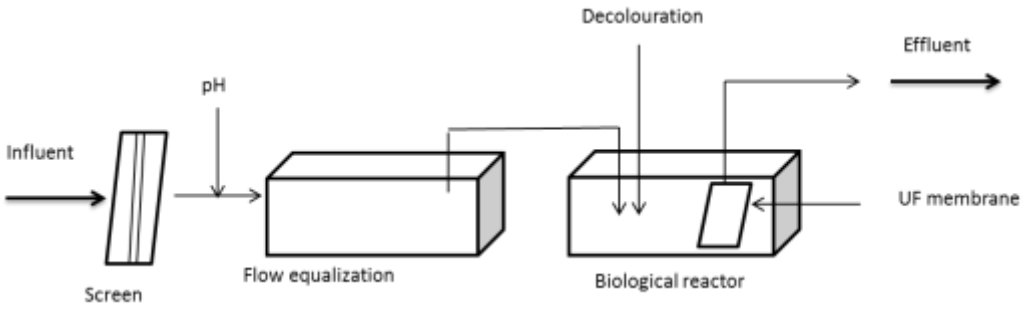

Figure 1.9. Membrane bioreactor[2].

The membrane bioreactor treatment combines the biological degradation process by activated sludge with a direct solid-liquid separation by membrane filtration, which their pore sizes ranging from 0,005 to 0,4 µm (micro or ultra-filtration membrane technology)[33].

Summarizing, the general characteristics of the most common kind of textile wastewater treatments plants described above are resumed in table 1.2.

Table 1. 2. Efficiency of the different textile wastewater treatment plants

Treatment processes of textile effluents					
Process	**% removal**				
	COD	**BOD**	**SS**	**COLOR**	**COST**
Activated sludge	80-93	90-98	50-95	20-50	Low
Activated sludge + decolorizing	80-95	90-98	50-95	80-95	Moderate
Chemical coagulation flocculation	60-80	60-80	90-95	90-95	High-moderate
Activated sludge + tertiary treatment	90-95	95-99	90-95	90-98	High-moderate
Percolating filter + chemical coagulation	85-95	95-98	90-95	90-98	Moderate
Combined urban water treatment	90-95	95-98	>90	80-95	Low
Membrane Biorector (MBR)	90-97	95-99	>99	80-98	Moderate

2. Objectives

The objective of this work is to study the application of metallic particles of metallic iron and magnesium-based amorphous alloy to the degradation of azo dyes.

In the work of Wang[26], it was reported that the $Mg_{73}Zn_{21,5}Ca_{5,5}$ metallic glass powders have good ability in degrading azo dyes. Their degradation efficiency was about 1000 times higher than commercial crystalline Fe powders. Moreover they were reported that high Zn content in the amorphous Mg-based enabled a greater corrosion resistance in water and higher reaction efficiency with direct blue 6 dye compared to crystalline Mg.

Similarly, we decided to evaluate the application of $Mg_{70}Zn_{30}$ metallic glass powders in to the degradation process of azo dyes and compare these results with Fe metallic powders.

Therefore, the main objective of this study is to prove the effect of different metallic alloys in the degradation of organic compounds in a wastewater treatment process. The main steps realized in the work are described below:

1. Production of non-crystalline metallic particles by melt spinner and mechanical grinding.
2. Design of the work method to obtain the degradation reaction of the contaminants in the laboratory.
3. Qualitative evaluation of the contaminants degradation reaction for every kind of metallic particles at different pH and temperatures.
4. Kinetic study of the reaction of contaminants degradation.

3. Materials and Methods

In this study we worked with two types of metallic particles. Commercial crystalline zero-valent iron and partially amorphous magnesium-zinc alloy.

3.1. Production of metallic particles

3.1.1. Synthesis of rapidly cooled metallic ribbons

The ribbon production was intended in order to produce amorphous $\mathrm{Mg_{70}Zn_{30}}$ alloys. In order to bypass the crystallization of the metallic liquid below the melting temperature, the solidification of the alloy was performed by melt spinning.

The ribbon production was intended in order to produce amorphous $\mathrm{Mg_{70}Zn_{30}}$ alloys. In order to bypass the crystallization of the metallic liquid below the melting temperature, the solidification of the alloy was performed by melt spinning.

Firstly, the weight of every compound was calculated to obtain of the desired $\mathrm{Mg_{70}Zn_{30}}$ composition, as it is shown in equation 3.1 . For this is necessary to know the total volume (V_T), the desired atomic % composition (at%) of each component and the atomic volume (V_A) for each element. Knowing the above values the total number of moles (N_t) can be calculated. The total volume used in this case was 1.5 cm^3,but it can be changed depending on the amount of ribbons to obtain.

$$N_t = \frac{(V_{Mg} \cdot \%\ \mathrm{Mg} + V_{Zn} \cdot \%\ \mathrm{Zn})}{V_t} \tag{3.1}$$

Subsequently, the necessary weight of each element (W_A) was calculated to obtain ribbons with the desired composition, as it is shown in equation 3.2 . In addition to the above values, it is necessary to know the atomic mass for each element (M_A).

$$W_A = N_t \cdot \mathrm{at\%} \cdot M_A \tag{3.2}$$

All mentioned values are summarized in Table 3.1. And the theoretical weight values were calculated for obtaining ribbons with the exact $\mathrm{Mg_{70}\ Zn_{30}}$ composition.

Table 3. 1. Data for the ribbons synthesis.

	Mg	Zn
V_A (cm³/mol)	14	9,16
M_A (g/mol)	24,305	65,409
at %	70,00%	30,00%
V_t (cm³)	1,5	
N_t	0,119540963	
W_A (g)	2,03381	2,345716

First of all, magnesium bar was cut by pliers in pieces. And zinc pieces were weighted by precision balance directly. And the weighted quantities of zinc and magnesium were placed inside a crucible homogeneously in order to be used in the melt spinner device.

Melt spinner is an equipment that permits the ultrarapid solidification of metallic alloys. The initial alloy is put inside a fused silica crucible with a nozzle at the bottom. The crucible is placed inside a coil (induction furnace) where the metallic sample is heated by induction of electric currents. The induction current heats the sample and it melts. When the melt reaches the desired temperature, an overpressure is applied inside the crucible and the liquid is injected on a rotating copper-beryllium wheel producing ribbon-shape samples. The high thermal conductivity of the copper and the thin thickness of the ribbons results in cooling rates of the order of 10^6 K/s. A scheme of the melt spinner device is shown in Figure 3.1. In order to avoid oxidation of the metallic samples, the process is performed under vacuum or inert atmosphere. Picture of crucible inside the coil and the cooper beryllium wheel is shown in Figure 3.2. Also, picture of chamber gas and tube of equipment are shown in Figures 3.3. and 3.4.

As a consequence of the ultrarapid cooling rate, atoms of certain metallic composition are not able to arrange in a crystalline state. The lack of crystalline growth during the solidification process results in a solid non-crystalline material. These materials are called amorphous alloys or metallic glasses, and they have a disordered atomic-scale structure similar to the one expected in the liquid state.

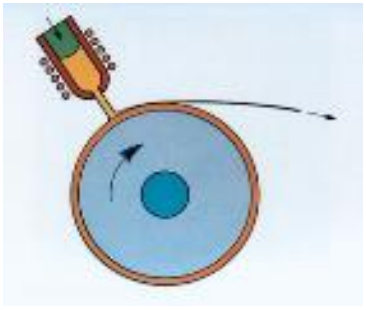

Figure 3. 1. Melt spinner diagram

Figure 3. 2. Melt spinner picture. The crucible with the sample inside the coil. Under of it is the cooper wheel.

Figure 3. 3. Chamber gas.

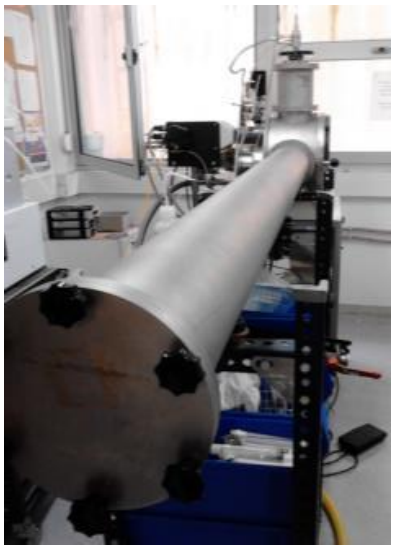

Figure 3. 4 tube, where the formed ribbons are collected.

3.1.2. Ribbon characterization

Topography and composition of the produced ribbons were analyzed by Focused Ion Beam Zeiss Neon40 Scanning Electron Microscope (SEM).The structure was analized by Bruker D8 Advance X-ray Diffraction (XRD). These equipments are in The Center for Research in Nanoengineering (CRnE) in UPC.

SEM is a type of electron microscope that produces images of a sample by scanning it with a focused beam of electrons. The electrons interact with atoms in the sample, and the reflected beam of electrons is collected, and then displayed at the same scanning rate on a cathode ray tube. It provides information about the sample's surface topography and composition. SEM can achieve magnifications ranging from 10 to in excess of 50000 times[29]. The composition analysis is performed by Energy-dispersive X-ray spectroscopy (EDS) using the X-ray emission generated due to the interaction of the electronic beam with the sample material.

Ribbons with the nominal composition $\mathrm{Mg_{70}Zn_{30}}$ in atomic percentage were checked by SEM. However some C, Si and other impurities or contaminations were detected by EDS. The presence of these elements on the ribbon surface is associated to contamination from the crucible or from sample manipulation. For this reason, the compositions in atomic percentage were normalized:

$$total\ at(\%)\ normalized = \frac{(\%Total - (\%\mathrm{C} + \%\mathrm{O} + \%\mathrm{Si} + \mathrm{Fe})}{\%\ Total} \cdot 100 \qquad (3.3)$$

The XRD is a technique used for identifying the atomic and molecular structure of a crystal. When a beam of X-rays impinges on a solid material, this beam will be diffracted in all directions.

Diffraction occurs when a wave encounters a series of regularly spaced obstacles that are capable of dispersing the wave and have spacings that are comparable in magnitude to the wavelength. The diffractometer is used to determine the angles at which diffraction occurs. From this diffraction pattern, the mean positions of the atoms in the crystal can be determined, as well as their chemical bonds, their disorder and other information[29].

XRD diagram shows the relationship between the intensity of X-rays received and the corresponding angle of diffraction. A crystalline sample presents crystalline planes that have different crystalline interplanar distances and orientations. The crystalline XRD spectrum is characterized by peaks of intensity at certain angles. Instead, an amorphous sample does not have long range structure or crystalline planes. The corresponding XRD pattern does not show well-defined crystalline reflections but broad peaks typical of liquids, glasses and amorphous materials.

3.1.3. Synthesis of metallic particles

The $Mg_{70}Zn_{30}$ ribbons were milled in the Micromill P7 at Universitat de Girona (UDG) in collaboration with the materials and thermodynamics research group from the physics department. The containers were made of steel and the milling balls were of chromium–nickel alloy, as you can see in Figure 3.5. The micromill was operated at 450 rpm during 20 h under atmosphere of Argon gas in order to avoid oxidation as much as possible.

In addition, the commercial crystalline Fe particles were milled in order to homogenize the size of all particles. In this case the micromill was operated with the same parameters as for the $Mg_{70}Zn_{30}$ ribbons.

Figure 3. 5.UDG Micromill. This image shows the containers.

3.1.4. Particles characterization

First of all, as soon as the Micro-particles were obtained, their topography, composition and structure were analyzed by SEM and XRD. Secondly, the distribution of particle size and the average particle diameter was measured from the SEM images with the help of imaje j program. The Image j software was created by national institutes of health (NIH) in the US. Some filters of the Image J were tested in order to increase the contrast and enhance distinction between particles, although, finally, it was opted to work with the original image.

Horizontal and vertical diameter was measured. Then, for each particle the mean was calculated. Each SEM image has in the bottom, the equivalence of a pixel to length in nanometers. And the diameter of particles was calculated in nanometers with this relationship. Finally, descriptive statistics and histogram of particles were realized by Minitab program.

3.2. Experimental degradation

3.2.1. Azo dyes

In this work two azo dyes were used; methyl orange and Reactive Black 5.

In the university laboratories we have methyl orange dye that is used as pH indicator. First of all, we chose this dye to do experiments. However, pH solution acidified with HCl ≈1 M to pH=3 as turned turbid due to a presence of precipitate. Another trouble that with this dye is you cannot work between transition ranges, because it is unstable. For these reasons, methyl orange dye was rejected.

We were thinking about others dyes, like Blue azo dye, tartrazine dye and yellow FLW. However finally, we decided to use Reactive Black 5. Because, it was used in a project of UDG (Universitat de Girona), in order to compare results. For the same reason, to acidify the solutions we use acetic acid instead of HCl or formic acid.

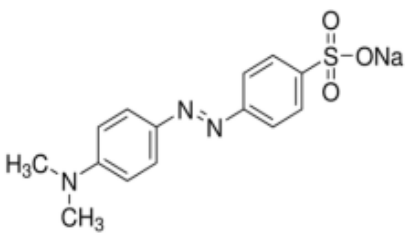

Figure 3. 6. The chemical structure of Methyl orange.[34]

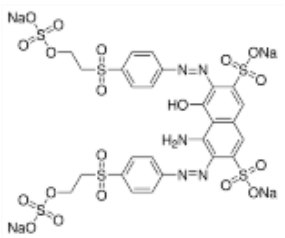

Figure 3. 7. The chemical structure of the Reactive Black 5[35].

3.2.1.1 Methyl orange

The methyl orange, as represented by the chemical structure in Figure 3.5, 4-[4-(dimethylamino)phenylazo]benzenesulfonic acid or orange III is an azo dye that forms orange or yellow crystals and is commonly used as an acid-base indicator, it is red below pH=3.1 and it is yellow above pH=4.4. It was used the same dye that it is used as an acid-base indicator.[34]

3.2.1.2 Reactive Black 5

Reactive Black 5 or Remazol black B, as represented by the chemical structure in Figure 3.6, is an azo dye that forms blue or black powders. It is classified within the Vinylsulphone Dyes[36], which are moderately reactive. The dyeing temperature is generally 60 ^{o}C and pH is 11.5 that get applied by utilizing a mixture of soda ash and caustic soda.[36] These dye show excellent fixation properties under proper alkaline condition[35].

3.2.2. Design of the dye degradation experiments

Based on previous work performed at the Universitat de Girona each tube was filled with 20 mL of 110 µM dye solution and 0.05 g of metallic powders. Except for the controls that were filled only with 20 mL of dye solution. To set the pH of the dye solution acetic acid or NaOH was used. Intial experiment showed that reactions were very solw in alkaline conditions.

The tubes were completely submerged in a thermostatic bath, in order to achieve a uniform temperature in all the parts of the tube. Several systems of tubes stirring were tested, as a proper agitation is very important for the correct development of the experiment. The best system is one in which the tubes are perpendicular to the direction of support movement. Finally, a device made with a wire mesh, which had a set of spacers to allow the water flow, was chosen. Other stirring systems, as this seen in figure 3.8. ,did not prevent the solid sedimentation or allow one to control the temperature.

Figure 3. 8. Stirring systems. Left) system which did not work. Right) System of agitation that it was used.

The thermostatic baths allowed to select the temperature. Moreover different kinds of tubes were tested. The initial polystyrene tubes showed many losses during the trials, as can be seen in Figure3.10. Afterwards, polypropylene and glass tubes were tested. They used to have some loss of solution and depositions of particles were observed in the walls. Finally, glass centrifuge tubes were tested and they had not loss of solution. Also, sometimes some depositions of particles were observed in walls. Different kinds of tubes can be seen in Figure 3.9. The glass tubes were the best option to do the experiments.

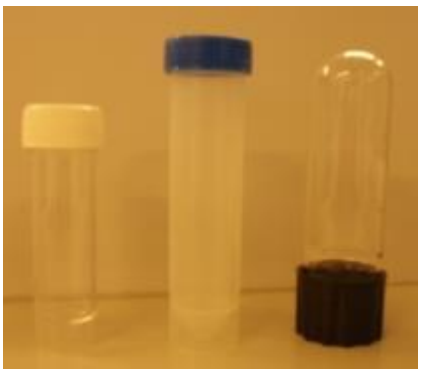

Figure 3. 9. Left to right: Polystyrene tubes, polypropylene tubes and glass centrifuge tubes.

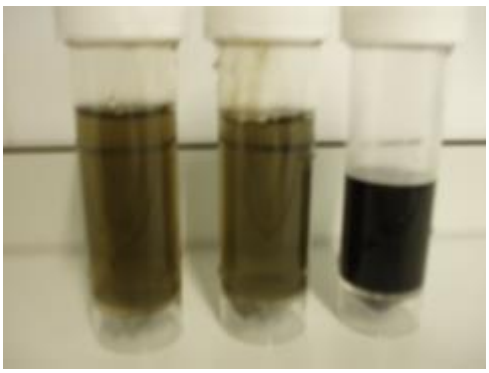

Figure 3. 10. Volume differences in tubes are observed due to the inlet and outlet liquid.

In order to monitor the degradation reaction, several tubes were left in the stirring device, each one during a specific time at constant stirring and temperature. Before to measure the absorbance , the reaction was slowed by basification with NaOH solution, the amounts of NaOH required to basify are summarized in Table 3.2.

Table 3. 2. Summary of NaOH quantities required to slow the reaction

pH solution	Alkaline solution added	Final pH
≈3	10 drops 1 M NaOH (≈ 2mL)	≈ 6.5
≈4	80 µL 0,1 M NaOH	≈6.5
≈5.6	60 µL 0,1 M NaOH	≈10
≈7	40 µL 0,1 M NaOH	≈10

The next step was to separate the solution of particles in order to make a correct lecture of the absorbance in the spectrophotometer. Firstly, a vacuum filtration was tested. However the dye was retained in the filter paper. Then, a Nylon syringe filter 0,45 um pore Scharlau 25 mm of diameter was tested, but it absorbed all the color. Finally, a PVDF syringe filter 0,45 µm pore Scharlau diameter 25mmwas tested. In this case, when 15 mL of solution were filtered almost the same absorbance value of the unfiltered solution was obtained. For some experiments it was opted to use this separation methodology, previously saturating the filter with 20 mL of the solution, the filter is shown in Figure 3.11. However, some odd and erroneous lectures of absorbance were attributed to the filtration technique and, finally, it was decided to use centrifugation as the separation technique, the device is shown in Figure 3.12. To centrifuge was use a Rotanta 460r centrifuge.

Solutions were filtered by a 0,45 µm pvdf filter. Previously it was saturated with the same solution. The syringe and filter were washed by each solution with ≈ 4 mL of solution two times and finally the filtered solution was analyzed by the spectrophotometer.

Figure 3. 11. Pvdf filter saturated with dye solution.

Centrifuge was worked during 15 min at 3000 rpm. High velocity were not tested for the danger that the glass tubes could exploit. The equipment is shown in Figure 3.12.

Figure 3. 12. Centrifuge

After separation of the micro-particles from the solution, the degree of dye degradation was measured by reading the absorbance in spectrophotometer.

During this project, pH electrode were changed. Because, the crison 5014T[37] pH electrode in the chemistry labs are for clean solutions (practically water). And we worked with a dirty solutions. Finally, the internal membrane of pH electrode was dyieng . And many troubles with calibrations and mesuraments were happened. For this, we chose crison 5021 T[38] electrode of pH, that permit to work with a difficult samples.The difference between two electrodes is shown in Figure 3.12.

Figure 3. 13. At left 5021T electrode and right the 5014T electrode. The 50-21T electrode has a circle.

Finally, from the results of all the tests realized and the available material in the laboratory we decided that the best experimental design was the one resumed in figure 3.12.

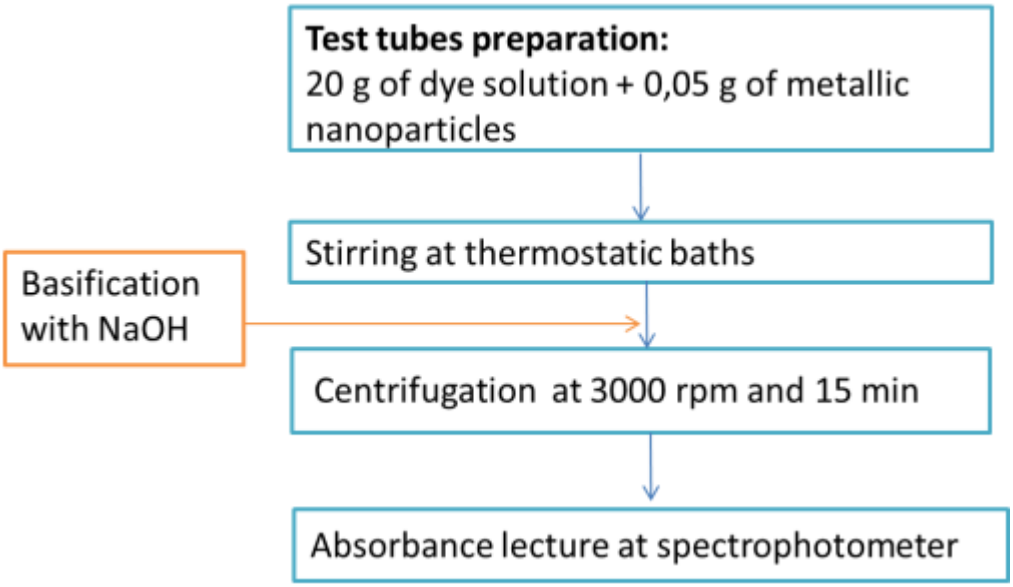

Figure 3. 14. Diagram of the best working procedure

3.2.3. Absorbance measurements

To study degradation process, first a visual control of decolouration process was done, in order to know the time of the degradation experiments. Then, we studied the reaction process at certain point of time.

Before the studies of decolourization, a serial of diluted of dye neutral solution were prepared in order to do the calibration curve at 597 nm. 597nm was the wavelength of maximum absorbance for Reactive Black 5. The calibration cruve was realized between 0,1 and 1 absorbance

To study the kinetics of the degradation process, the absorbance of the solution in each tube was analyzed at a certain point of time. Each study was realized at specific temperature and pH.

It is possible to know the concentration of dye for each absorbance, when the calibration curve and the linear equation is obtained . If we have a first order kinetics, the rate constant be able to obtain from the slope representing the logarithm of the concentration (lnC) vs time.

3.2.3.1. Beer & Lambert law

Each molecule has the ability to absorb its own characteristic frequencies of the electromagnetic radiation. This process transfers energy to the molecule and causes a decrease on the intensity of the incident radiation.

The spectral domain of the UV/Visible is well known because it includes the visible part of the spectrum and is widely used in quantitative analysis. Measurements are based on the Beer-

Lambert law, which relates the absorption of light under certain conditions to the concentration of a compound[39].

Light incident on a sample (I_0) can be reflected, absorbed, or transmitted. The ratio of light transmitted through the sample to the light incident on the sample $\frac{I}{I_0}$, is defined as the transmittance throught the sample (T). Absorbance (A) can be calculated from transmittance using the following relationships 3.4, 3.5 and 3.6

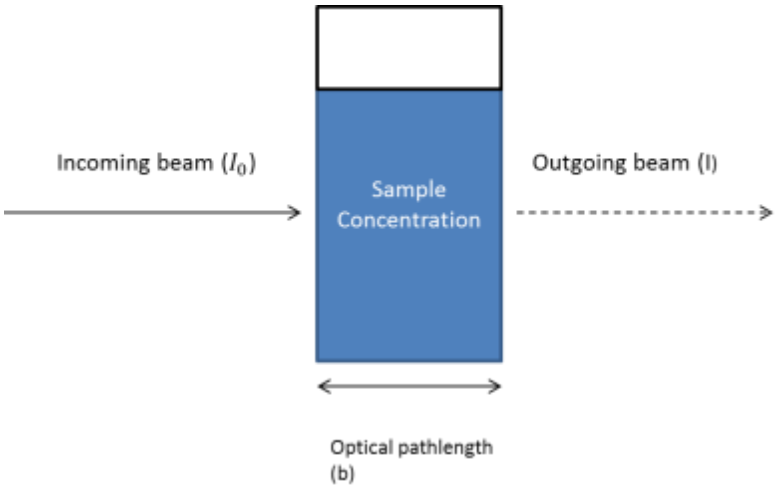

Figure 3. 15. Diagram of beam trough the sample.

$$T = \frac{I}{I_0} = 10^{-kcb} \tag{3.4}$$

$$\%\,T = \frac{I}{I_0} * 100 \tag{3.5}$$

$$A = -\log\frac{I}{I_0} = kcb \tag{3.6}$$

Samples are routinely measured in absorbance because it is proportional to the concentration of the sample (c) (Beer's law). And it is proportional to the optical path length (Bouguer's law).). At a given wavelength, the proportionality constant (k) is unique for any specie. When the optical path length (b) is 1 cm and the sample concentration is 1 mole/L, the proportionality constant (k) for a given species becomes the molar absorptivity (ε) yielding the more commonly seen equation relating absorbance and concentration[39,40] .

In a Dual-Beam design, as you can see in figure3.12, the monochromatic light coming from the monochromator is divided into two paths using either a rotating sector mirror or a semi-transparent beam-splitter. The split light beam is passed through the sample compartment in two

paths, one passing through the sample cell and the other passing through a reference cell. After passing through the sample compartment the beams are focused onto the detector. In a dual-beam system a baseline measurement (with distilled water) is acquired prior to sample analysis. This is the spectral information that is rated against the sample beam to calculate transmittance. In addition, in a dual-beam system, the reference beam is also rated against the sample beam. This second comparison serves to compensate for any variation in temperature, voltage, or lamp intensity that may occur as the measurement is acquired. The result is a very accurate and stable acquisition of the sample spectrum over the full wavelength range. In this case the transmittance is obtained with the expression 3.7[40]:

$$\%\,T = \frac{\frac{I_{sample\ (\lambda)}}{I_{Reference\ (\lambda)}}}{\frac{I_{Baseline\ sample\ (\lambda)}}{I_{Baselline\ reference\ (\lambda)}}} 100 \qquad (3.7)$$

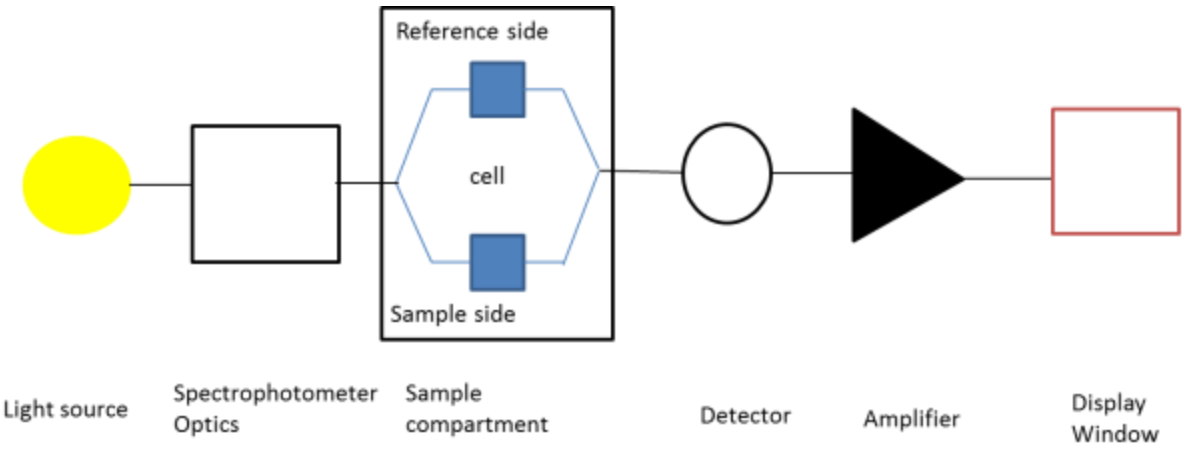

Figure 3. 16. Basic layout of a double-Beam Spectrophotometer. [40]

Absorbance measurements of this work were carried out with a Shimadzu 2600 UV-visible spectrophotometer. We use UVprobe software to work with the spectrophotometer. It is multifunctional software supplied as standard with Shimadzu UV-VIS Spectrophotometers.

In the method of the program we were choose a direct measure of the absorbance, lectures every 1 nm and a fast velocity to do the lectures. Before, other velocity was tested. However final results were the same.

Before each group of absorbance lecture, a baseline and a zero with distilled water were realized by the spectrophotometer.

Decolourization measurements (D) was calculated from the initial concentration (c_i) and dye concentration at time t (c_t) by measuring the absorbance at the visible maximum dye absorption wavelength, as it is shown in equation 3.8. In this case was 597 nm for Reactive Black 5.

$$D(\%) = \frac{(c_i - c_t)}{c_t} \cdot 100 \tag{3.8}$$

4. Results and dicussion

Results are structured in two parts: section 4.1 is focused on the study of particles. In the second part(section4.2) is focused on the study of colour degradation.

4.1. Production of metallic particles results

4.1.1. Synthesis of rapidly cooled metallic ribbons results

Magnesium and zinc were weighted in order to synthesize $Mg_{70}Zn_{30}$ .The weights for each component are summarized in Table 4.1. As it is shown in the table, composition of ribbons is the one that was desired to obtain.

Table 4. 1. Weigh and theoretical percentage of atomic composition for each sample

Sample	Weigh Mg (g)	Weigh Zn (g)	Theoretical % at. Mg	Theoretical% at. Zn
1	2,0837	2,418	69,36%	30,64%
2	2,0456	2,3604	69,99%	30,01%
3	2,048	2,3967	69,69%	30,31%
Mean	2,0591	2,3917	69,68%	30,32%

The synthesis conditions used in the solidification process by the melt-spinning are resumed in Table 4.2 for each one of the samples produced.

Table 4. 2. Parameters used for the production of $Mg_{70}Zn_{30}$ ribbons.

Parameter	Sample 1	Sample 2	Sample 3
Temperature (ºC)	910	730	820
Chamber pressure (mbar)	400	500	400
Injection pressure (mbar)	800	800	800
Wheel velocity (m/s)	40	40	40
Thickness crucible-wheel(mm)	1	1	1

Looking the data in Table 4.3, and comparing to the melting points of the metallic components of the alloy (Table 4.4), the temperature reached during the synthesis of the ribbons should be enough for a correct synthesis.

Table 4. 3. Melting point of magnesium and zinc

Element	Mg	Zn
Melting point(ºC)[41]	650	419,53

Finally, the ribbons and some powders were collected and weighted. The results are summarized in Table 4.4. The powders were excluded because they may contain some contamination, such as pollutants of other alloys previously produced in the same solidification equipment.

Table 4. 4. Product of synthesis.

Sample	1	2	3
Powder weigh (g)	1,26444	1,06046	1,2956
Ribbons weigh (g)	1,69	1,49755	1,5765
Total (g)	2,95444	2,55801	2,8721

The ribbons corresponding to sample 1 were apparently normal, but little quantity of ribbons was collected. For this in the synthesis of sample 2, the pressure difference was reduced. However, lower temperature was achieved and some spherical particles and strange pieces were observed. In the case of sample 3, some ribbons were a bit more fragile and fragmented.

4.1.2. Ribbons characterization

4.1.2.1 SEM results

Morphology surface and percentage of atomic composition were checked by SEM.

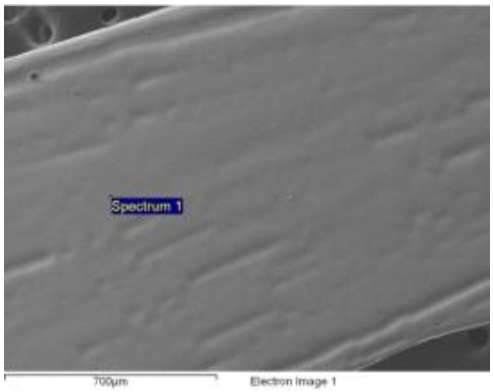

Figure 4. 1 Morphology surface of sample 1

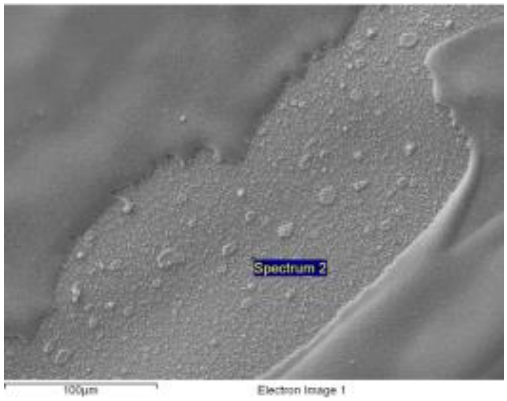

Figure 4. 2. Morphology surface of sample 3.

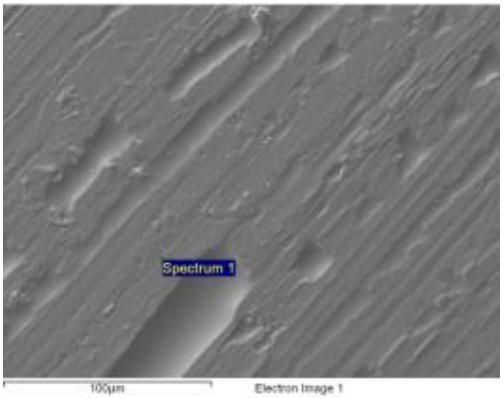

Figure 4. 3. Morphology surface of sample 2 on the side of the ribbon contacting the copper wheel.

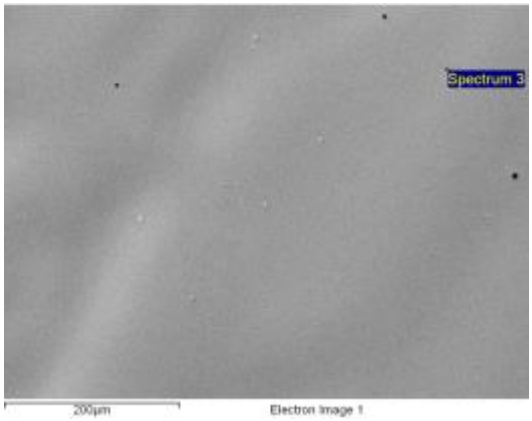

Figure 4. 4. Morphology surface of sample 3.

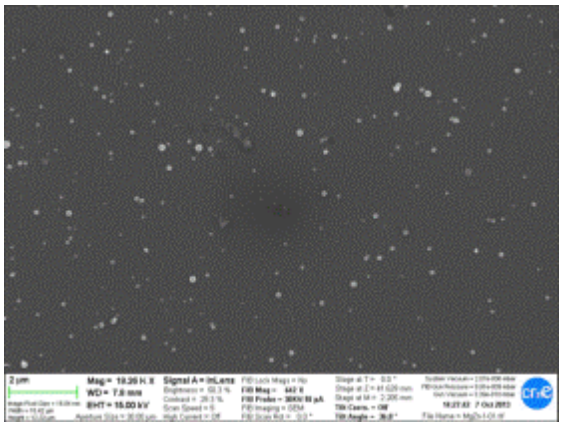

Figure 4. 5. Enlargement of morphology surface of sample 3.

The SEM inspection of the surface of the ribbons produced by melt-spinning allows a quick examination of the quality of the ribbons as well as the examination of the composition of the material after the solidification process. The two surfaces of the ribbons show very different characteristics, the upper side shows a smooth liquid-like surface while the side in contact with the cooling copper wheel during the solidification shows the scratches due to the impact on the wheel (Figure 4.3). Topography of ribbons 1 and 3 were apparently normal, as it is shown in Figure 4.1 and Figure 4.4. However, for sample 3, some spherical parts were observed, when the image of ribbons were enlarged as it is shown in Figure 4.5. Ribbons of sample 2 had a strange morphology surface, some parts of the ribbons had different topography as it is shown in Figure 4.2.

The composition of the ribbons of sample 1(SAP1), sample 2(SAP2) and sample 3(SAP3) were analyzed by SEM. Some points of ribbons were chosen on either side. Then, the average for each of the measured elements was done. The percentage of normalized sample was calculated (with equation 3.3) and it is shown in Table 4.5.

Table 4. 5. Results of atomic compositions were obtained by SEM for the MgZn ribbons.

Ribbons	% at. O	% at. Mg	% at. Si	% at. Zn	% at. total	% at. normalized total	% at. normalized Mg	% at. normalized Zn
Mean sample 1	0,00	64,02	0,69	28,94	100,00	92,96	68,86	31,15
Mean sample 2	1,155455	59,78	0,54	27,48	100,00	87,25	68,40	31,60
Mean sample 3	1,25	68,22	0,00	28,59	100,00	96,82	70,46	29,54
Total mean	0,80	64,01	0,41	28,34	100,00	92,34	69,24	30,76

As it is showed in Table 4.5 , the final composition were $Mg_{69,0}Zn_{31}$. This composition in atomic percentage was almost the same as we expected $Mg_{69,7}Zn_{30,3}$ .as it is shown in Table 4.1.

4.1.2.2 XRD results

Material structure was analyzed by XRD.

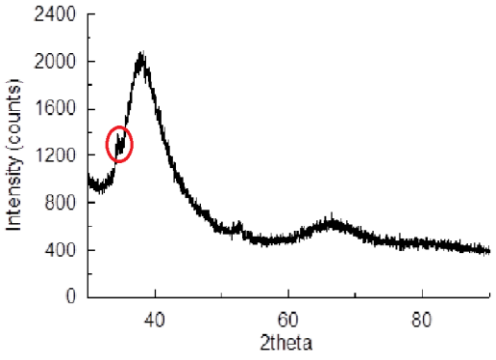

Figure 4. 6. XRD result of ribbons of sample 1. In red, peak that cannot identify.

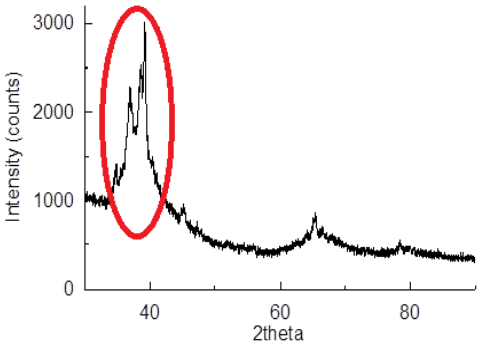

Figure 4. 7. XRD result of sample 2.

Ribbons of sample 1 were almost completely amorphous. As it is shown in Figure 4.6, some little crystalline peak is detected. However it cannot be identified. In contrast, ribbons of sample 2 and 3 were composed by amorphous fraction together with a $Mg_{51}Zn_{20}$ crystalline phase, as it is showed in Figure 4.7. This is a metastable phase, thermodynamically unstable at ambient pressure and temperature conditions. It forms a complex structure with many interconnected icosahedra[42].Probably this structure is closely to the liquid structure, this permitting an easy nucleation of the crystallites.

Differences between the synthesis method, especially with temperatures were achieved in different samples. It had caused the differences between the structures of the obtained materials.

4.1.3 Particles characterization

4.1.3.1 SEM results

MgZn particles

Sample 1, sample 2 and sample 3 were mixed and milled. When the sample was checked after the milling process, big pieces of metal were observed and some quantities of powder too. The big pieces were rejected.

Then also the percentage of atomic composition and surface morphology of Fe particles and MgZn particles were ascertained by SEM, as it is shown in Figure 4.8.

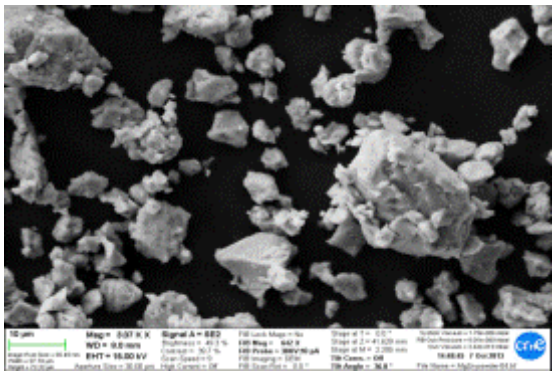

Figure 4. 8. Morphology surface of MgZn particles were obtained by SEM.

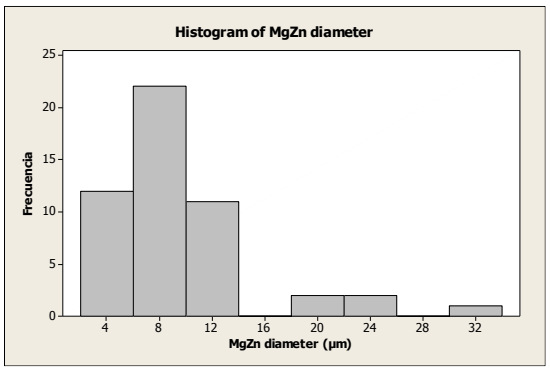

Figure 4. 9. Histogram of MgZn diameter

The histogram in Figure 4.9 shows the distribution of frequency for the diameters of the particles obtained after the milling process.

Table 4. 6. Descriptive statistics of MgZn particles diameter

N	Mean	Standard error of the mean	St Dev	Variance	VarCoef
50	9,53	0,8837	5,919	35,039	62,11
Minimum	**Maximum**	**Q1**	**Median**	**Q3**	**IQR**
3,692	33,943	6,1913	7,563	10,63	4,436

Average diameter of MgZn particles was 9,53 µm, as it is showed in Table 4.8 and Figure 4.9.

The atomic composition of MgZn powder was obtained by SEM and it is resumed in Table 4.7. The percentage of atomic composition normalized (excluding other elements than Mg and Zn) is resumed in Table 4.10.

Table 4. 7. Percentage of atomic composition of MgZn powder for each point

Point	C	O	Mg	Si	Fe	Zn	Total	% at normalized total
1	-	7,19	60,70	0,51	-	31,6	100	92,30
2	-	24,43	49,53	0,41	-	25,64	100,01	75,16
3	7,33	42,06	36,60	0,35	0,2	13,47	100,01	50,06
Mean	7,33	24,56	48,94	0,42	0,2	23,57	100,01	72,51

Table 4. 8. Normalized composition of MgZn powder.

Point	% at normalized Mg	% at normalized Zn
1	65,76	34,24
2	65,90	34,11
3	73,10	26,91
Mean	68,26	31,75

Atomic normalized composition was $\mathrm{Mg}_{68,2}\mathrm{Zn}_{31,8}$. However in some points huge amounts of oxygen were detected, as it is shown in Table 4.7.

Fe particles

The Fe particles were produced with similar milling conditions than the ones used for the MgZn alloy. The SEM inspection of the Fe-Powder and the calculated size distribution are shown in Figures 4.10 and 4.11 and Table 4.9.

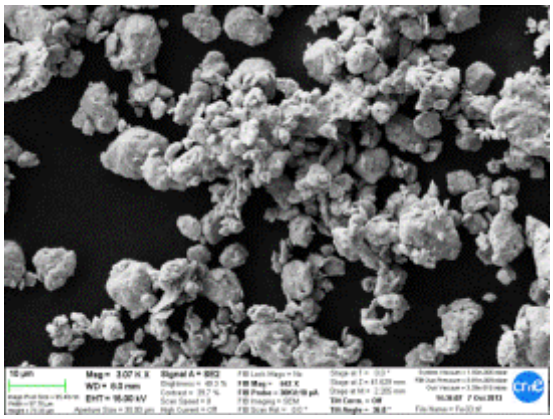

Figure 4. 10. Morphology surface of Fe particles.

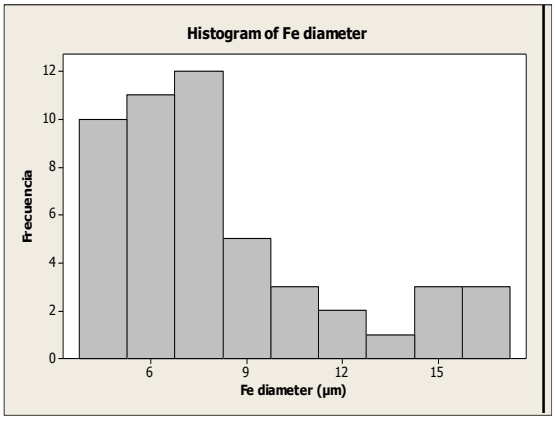

Figure 4. 11. Histogram of Fe particles diameter.

Table 4. 9. Descriptive statistics of Fe particles diameter

N	Mean	Standard error of the mean	St Dev	Variance	VarCoef
50	8,189	0,494	3,491	12,189	42,63
Minimum	**Maximum**	**Q1**	**Median**	**Q3**	**IQR**
3,811	16,436	5,568	7,325	9,558	3,99

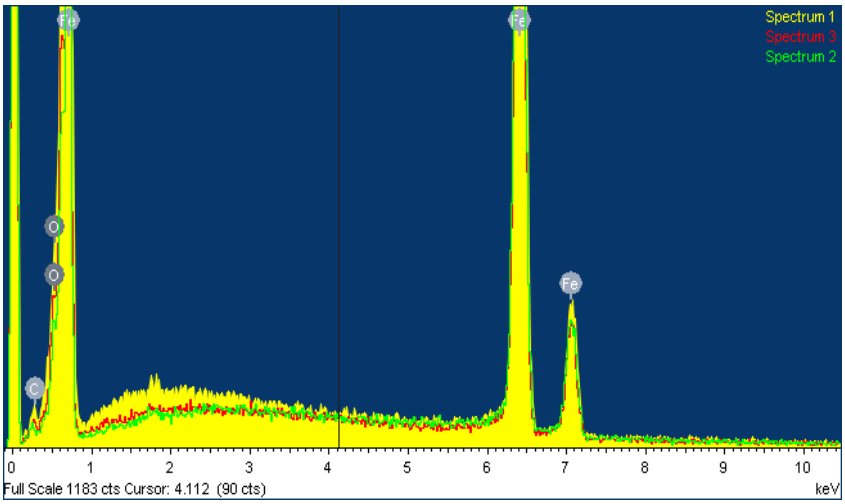

Figure 4. 12. EDS spectrum for Fe particles.

The average diameter for commercial Fe particles was 8,19 µm. It is smaller than MgZn particles, which was 9,53 µm, but it is perfectly. The EDS spectrum for Fe particles, as it is represented in Figure 4.12, shows some impurities of carbon and oxygen.

4.1.3.2 XRD results

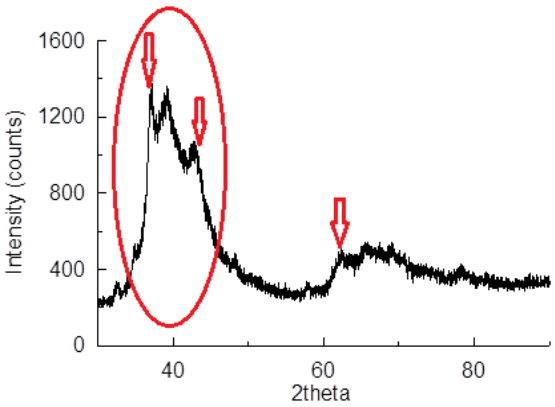

Figure 4. 13. XRD results for MgZn particles. The arrows show the crystalline reflections corresponding to magnesia (MgO).

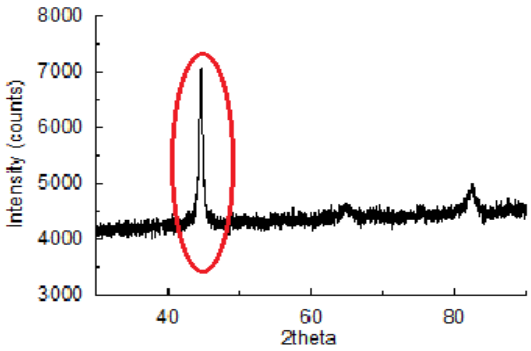

Figure 4. 14. XRD results for commercial Fe particles

The X-ray diffraction patterns of MgZn ribbons can be interpreted as follows. As it shown in Figure 4.13, $Mg_{68,2}Zn_{31,8}$ particles, similarly to the ribbons of samples 2 and 3 show a partially amorphous structure with a $Mg_{51}Zn_{20}$ crystalline phase. However, in addition to the phases already present in the ribbons, the presence of MgO was detected by XRD in the MgZn particles. The presence of MgO is indicated by arrows in Figure 4.13. On the other hand, as we can see in the figure 4.14, the Iron particles only show crystalline peaks related to the bcc phase of Iron (ferrite). This indicates iron particles are clearly crystalline, however, the width of the peaks indicates a very small size of the crystalline grains inside the powder micro-particles.

Also, when $Mg_{70}Zn_{30}$ were milled. MgO was detected by XRD. It is a trouble, because Mg probably were not zero valent. It is necessary , because when Mg zero-valent were oxidized, they can react and broken the N=N bond. For this, $Mg_{70}Zn_{30}$ particles were not effective to degrade azo dye. The process lasted for many weeks at pH=7 and 10 and high temperatures (41°C) and 4 days at pH=3 and 41°C.

4.2 Absorbance measurements

The lecture of absorbance of a series of diluted dye solution was carried out in order to do a calibration curve. The calibration curve will allow us to transform the values of measured absorbance into dye concentration. The result is shown in Figure 4.15. The dye solution had a pH≈6.5 in that case.

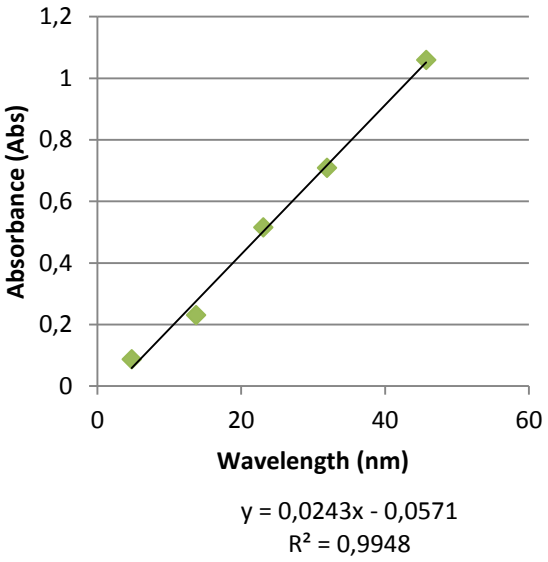

Figure 4. 15. Calibration curve 597 nm of Reactive Black 5, at pH≈6.5.

A good value of R^2 was obtained, as it is shown in Figure 4.15.

4.2.1 Dye degradation with MgZn Micro-particles

Several experiments were carried out with MgZn particles. However they were rejected due to their reaction was slow at high temperature (41^{o}C) and low pH medium (pH=3) . By eye inspection, it needed 4 days and 4:30h to achieve a similar degradation as the one obtained using iron only in 45 minutes. In Figure 4.16 we can observe the colour change. The first tube was the control, it had a dark blue color, The second tube was the dye degradation by MgZn during 4 days end 4.30 hours had a light blue/ lilac colour and the third tube was the dye decolouration by Fe in 45 minutes, it has a light brown/red coloration.

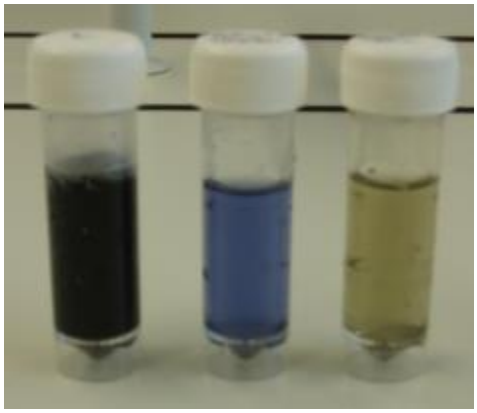

Figure 4. 16 From left to right: Control tube, reactive Black 5 with MgZn, reactive black 5 with Fe.

Experiments at 41 ^{o}C and different pH (3,7 and 10) were prepared by MgZn particles. However, most of the tubes used show some degree of leaking and, therefore, the results were rejected.

4.2.2 Dye degradation with Fe

In this section the results of the dye degradation using Fe particles and different pH and temperature conditions will be described.

pH ≈ 7, T = 41^{o}C, polypropylene tubes and filtration

These experiments were carried out at pH = 7 and 41 ^{o}C. Below the results obtained with Polypropylene tubes and filtration with pvdf filter as separation method are shown in Table 4.10 while results obtained with glass tubes and filtration with pvdf filter as separation method are shown in Table 4.11.

Table 4.10. Results for each tube at pH=7, 41^{o}C. Using a polypropylene test tubes and filtration.

Tube	Dye solution weight (g)	Fe weight (g)	Reaction time (h)	Abs. at 597 nm	C (mg/L) of dye	lnC
Control	20,0314	0	53	3,844	160,5	5,08
13h	20,0340	0,0501	13	3,617	151,2	5,02
24h	20,0615	0,0508	24	2,828	118,7	4,78
30h	20,0363	0,0509	30	2,706	113,7	4,73

Table 4. 11.Results for each tube at pH=7, 41ºC. Using a glass test tubes and filtration.

Tube	Dye Sol. Weight (g)	Fe weight (g)	Reaction time (h)	Abs. at 597 nm	C (mg/L)	lnC
Control	20,0314	0	53	3,844	160,5	5,08
0h	20,0693	0,0509	0	3,838	160,3	5,08
1h	20,0281	0,0503	1	3,719	155,4	5,05
2h	20,0432	0,0509	2	3,715	155,2	5,04
4h	20,0383	0,0501	4	3,601	150,5	5,01
24h	20,0560	0,0503	24	2,537	106,8	4,67
53h	20,0788	0,0504	53	0,242	12,3	2,51

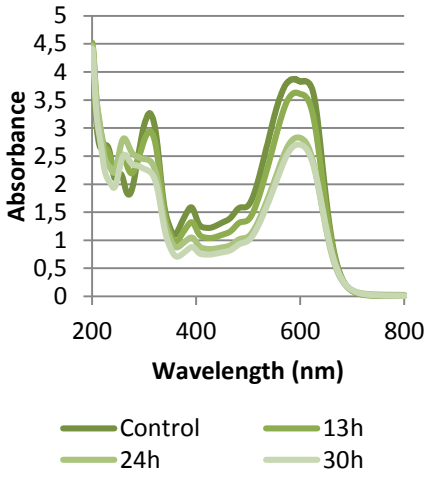

Figure 4. 17. . Evolution of UV-visible absorption spectra for each tube at pH = 7, 41°C. Using a polypropylene test tubes and filtration.

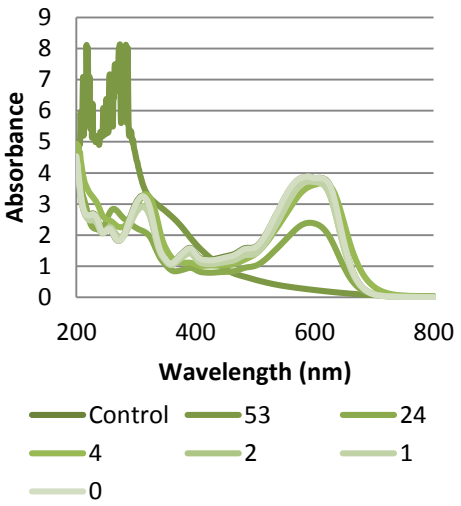

Figure 4. 18. . Evolution of UV-visible absorption spectra for each tube at pH = 7, 41°C. Using a glass test tubes and filtration.

As it is shown in Table 4.10 and Figure 4.17, the dye was decoloured at pH=7 and 41°C. But, only 29,2 % of dye was decoloured in 30 h. On the other hand, as showed in Table 4.11 and in Figure 4.18 dye for glass tubes was decoloured a 33,5% in 24 h.

Depositions of Fe were observed in the walls of test tubes. For this, results were compared at same time with glass tubes. Comparison between different kinds of materials is shown in Table 4.12 and Figure 4.19 at pH ≈7 and 41°C.

Table 4. 12. Comparison between results obtained with glass and propylene tubes, pH ≈ 6.5, 41 °C during 24 h.

Tube	Dye solution weight (g)	Fe weight (g)	Reaction time (h)	Abs. at 597 nm	C (mg/L) of dye	lnC
Glass	20,056	0,0503	24	2,537	106,8	4,67
Polypropylene	20,0615	0,0508	24	2,828	118,7	4,78

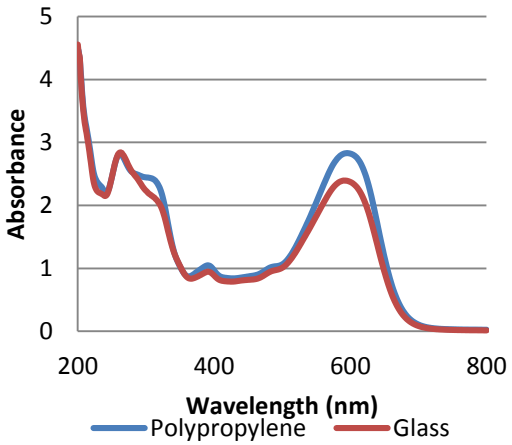

Figure 4. 19. Comparison between results obtained with glass and propylene tubes at pH≈6.5 and 41ºC

As it is demonstrated in Figure 4.19, dye solution in glass tube(34%) was more decolourated as compare to the dye solution in polypropylene tube(26,4 %).

Below all the results obtained with glass tubes and centrifugation as separation method. Filtration method was rejected because it could obtain values with a high error due to possible variations in the concentration.

pH≈3, 20ºC, glass tubes and centrifugation

The glass test tubes were prepared at pH=3 and 20 ºC. Before the lecture of absorbance were centrifuged . The results are shown in Table 4.13 and figure 4.20

Table 4. 13. Resume of results at pH=3, 20ºC. Using a glass test tubes and centrifugation.

Tube	Fe weight (g)	Dye solution weight (g)	Reaction time (min)	Abs. at 597nm	C(mg/L) of dye	lnC
Control	0	20,0415	64	3,837	160,0	5,08
1min	0,0508	20,0426	1	3,727	155,5	5,05
6min	0,0501	20,0520	6	0,654	29,0	3,37
8min	0,0508	20,0692	8	0,553	24,9	3,21
16min	0,0507	20,0080	16	0,389	18,1	2,90
20min	0,0505	20,0030	20	0,211	10,8	2,38
32min	0,0504	20,0339	32	0,209	10,7	2,37
38min	0,0509	20,0251	38	0,156	8,55	2,15
55min	0,0509	20,0077	55	0,124	7,23	1,98
64min	0,0501	20,0461	64	0,076	5,26	1,66

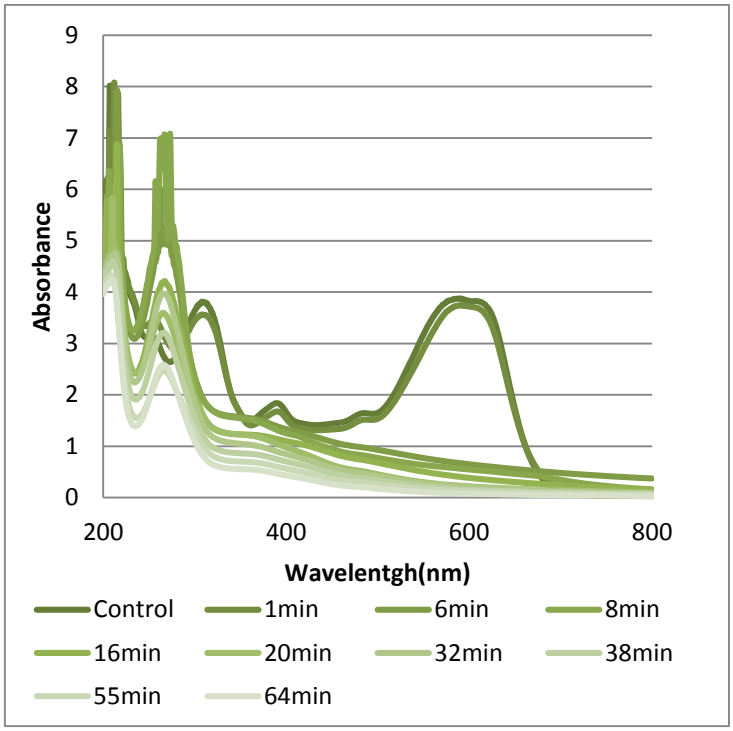

Figure 4. 20. Evolution of UV-visible absorption spectra for each tube at pH=3, 25°C. Using a glass test tubes and centrifugation.

At these conditions, the reaction was so fast. In less of 5 minutes the dye was decoloured totally. Kinetics study at pH = 3 was not possible with our experimental facilities, because it was so fast.

pH≈5.6, 25°C, glass tubes and centrifugation

Decolourization process at pH=3 and 20 °C was very fast. For this, decolourization was tested at pH≈5.6 and 25 °C, as it is shown in Table 4.14 and Figure 4. 21. The pH≈5.6 was the pH of the dye solution without adding acid or base.

Table 4. 14. Results of dye decolourization 25 °C and pH=5.6, using glass tubes and centrifugation.

Tube	Dye weigh(g)	Fe weigh(g)	Reaction time (h)	abs at 597 nm	C(mg/L)	lnC
0h	20,0438	0	0	3,847	160,7	5,08
11h	20,0278	0,0503	11,3	3,832	160,0	5,08
24h	20,0561	0,0501	24	3,823	159,7	5,07
46h	20,0239	0,0504	46	3,826	159,8	5,07

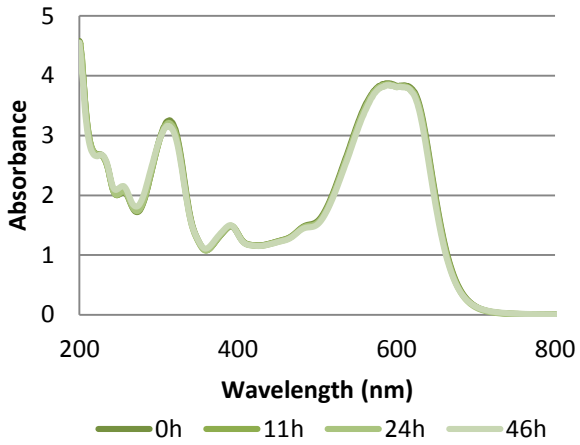

Figure 4. 21. Dye decolourization process at 25 ^{o}C and pH=5.6. Using glass tubes and centrifugation.

However in 2 days , any difference in decolourization were observed. Decolourization process at pH=5.6 and 25 ^{o}C was too slow. For this, pH parameter was changed by kinetics study and a solution of pH around 4 was chose to do the experiments.

4.2.3 Decolourization kinetics study of Reactive Black 5 dye by Fe

The study of the dye degradation kinetics was realized at pH=4.13 and two different temperatures: 25^{o}C and 41^{o}C. The absorbance curves and the corresponding calculated dye concentrations are shown in Table 4.15, Figure 4.22 and Figure 4.24 (T=25^{o}C) and Table 4.16, Figure 4.23 and Figure 4.25 (T=41^{o}C).

Table 4.15. Dye dregradation by Fe at pH=4 and 25ºC

Tube	Time (h)	Abs 597 nm	C (mg/L)	lnC
0h	0	3,83	159,9	5,07
1h	1	3,79	158,2	5,06
2h	2	3,77	157,5	5,06
3h	3	3,68	153,7	5,04
4h	4	3,64	152,1	5,02
13h	13	3,39	141,7	4,95
17h	17	3,33	139,22	4,94
24h	24	2,4	100,91	4,61
76h	76	1,41	60,374	4,10
98h	98	0,48	22,185	3,10

Table 4.16 Table 4. 17. Dye dregradation by Fe at pH=4 and 41ºC

Tube	Time (h)	Abs 597 nm	C (mg/L)	ln C
1h	1	3,834	160,1	5,08
2h	2	3,711	155,1	5,04
2,5h	2,5	3,603	150,6	5,01
3h	3	3,423	143,2	4,96
4h	4	1,874	79,47	4,38
5h	5	1,015	44,12	3,79

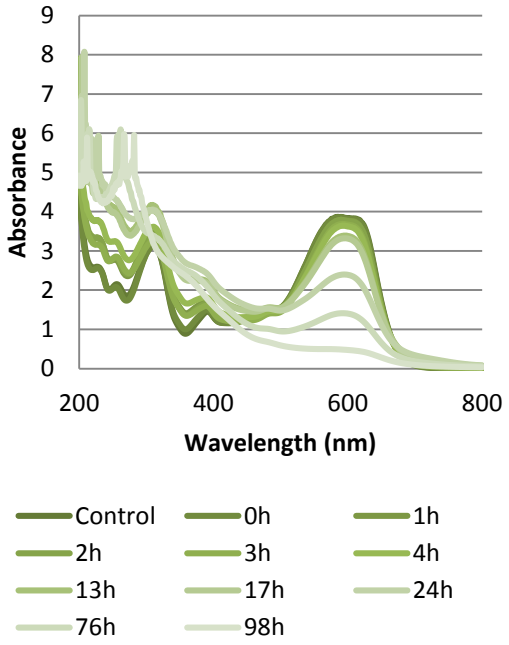

Figure 4. 22. Decolourization at pH=4 and 25ºC. Using a glass tubes and centrifuge.

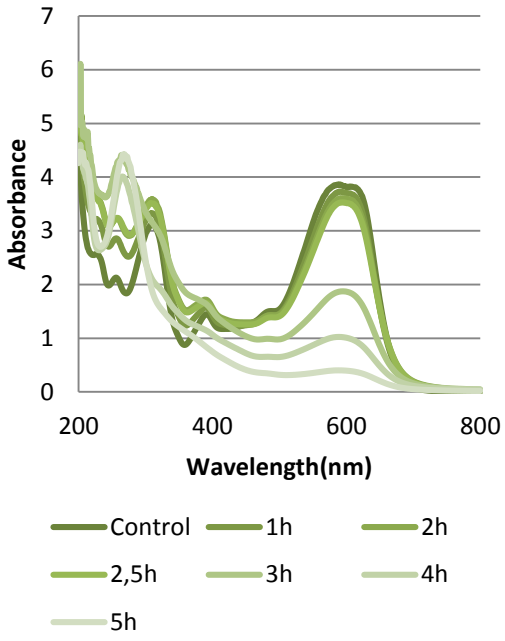

Figure 4. 23. Decolourization at pH=4 and 41 ºC. Using glass tubes and centrifuge.

For pH≈4 and a temperature of 41ºC the Reactive Black 5 decolouration needed around of 5h to reach a an almost complete degradation of the dye. On the other hand, at room temperature (25ºC), the Reactive Black 5 was decoloured by Fe in 98h (≈4days). As can be seen in these figures, when the dye was decoloured new peaks in the UV region appeared because inorganic compounds were formed. The peaks on the UV region are very similar in both cases, showing that the degradation reaction follows the same stages, although much more accelerated due to the increase of temperature.

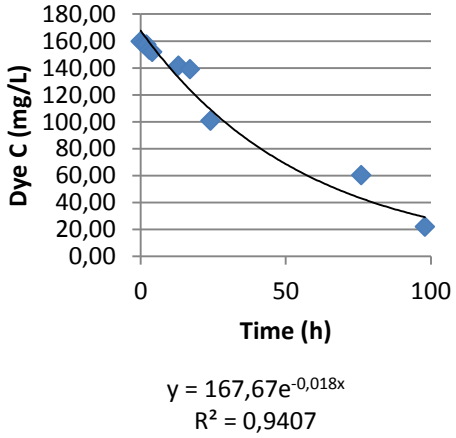

Figure 4. 24. Decolourization at 25ºC and pH=4. Solid line corresponds to a fitted exponential decay function.

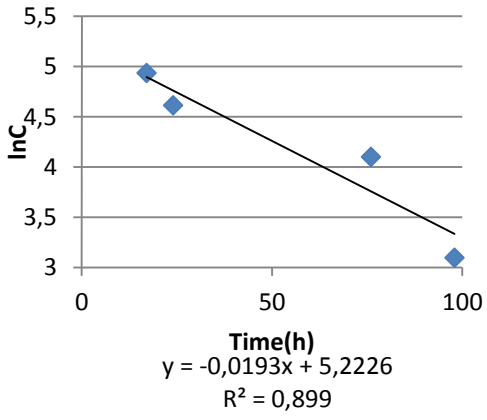

Figure 4. 25. lnC vs Time. Solid line corresponds to a fitted linear function.

As it is shown in Figure 4.25 , the kinetic constant was found 0,0193h^{-1} at pH=4 and 25^{o}C. To do the kinetics chart (Figure 4.25) there were used the values between 17h and 98 h in order to obtain a better adjustment. This procedure was needed because a lag phase was observed in the initial stage of reaction. This lag phase was observed in all the pH studies but in the cas of pH≈3.

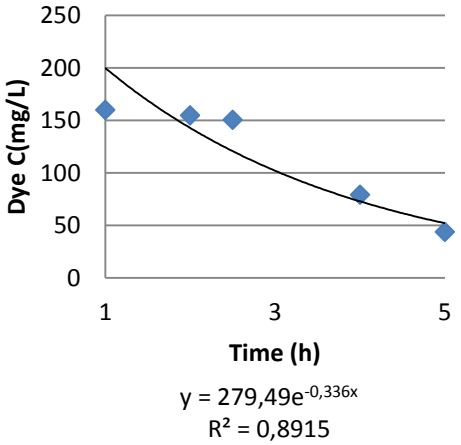

Figure 4. 26. Decolourization at 41^{0}C and pH=4. With a exponential line.

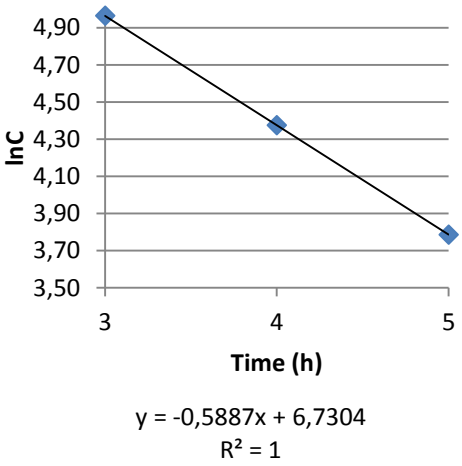

Figure 4. 27. lnC vs Time. With a linear line.

As it is shown in Figure 4.27, the kinetic constant was found 0,5887 h^{-1} at pH=4 and 41^{o}C. In this case, the kinetics were obtained using the values between 3h and 5h.

The spectra of decolourization by means sero-valent Fe, as it can be seen in Figures 4.17-4.23, demonstrate the cleavage of the azo bond and the formation of reaction products. When the azo dye was reduced, the azo double bond was destroyed and the absorbance caused by the azo group (at 597 nm) became progressively lower.

The best result to degrade the azo group was obtained by Fe particles at pH = 3 and 20 ^{o}C . On the whole, as expected, at higherer temperature and pH the reaction rate is faster, as it is shown in Figure 5.1 and Figure 5.2. However, from the results obtained here, in the conditions of pH and temperature feasible inwater treatment plants the Fe particles would show too low degradation effect.

4.3. Comparison of pH and temperature kinetics

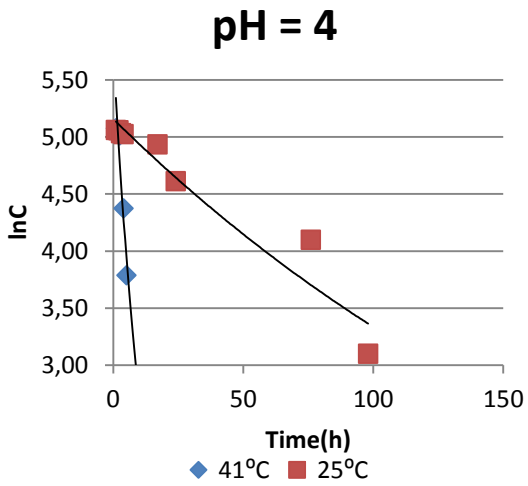

Figure 5. 1. Comparison of dye degradation at pH4 and different temperatures.

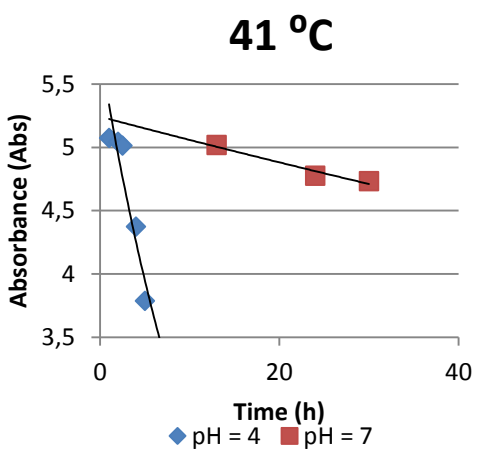

Figure 5. 2. Comparison of dye degradation at 41ºC and different pH.

In the kinetics studies it was observed that at first stages the reaction had a lag phase. This means that the iron is not directly reacting with the azo dye. This may be the reason why the kinetic constants are so low if compared with other studies. However, the majority of the studies reported results at pH=3, as it can see in Table5.1.

Table 5. 1. Resume of kinetics constants of Reactive Black 5 decolouration by Fe^0

pH	T(ºC)	(k)	R^2
4	41	0,5887 (h^{-1})	1[a]
4	25	0,0193 (h^{-1})	0,899[a]
3	20	0,146[b]-0,153[c](min^{-1})[12]	

[a] Rate constants obtained in this work. [b]Rate constants in anaerobic conditions and [c] aerobic conditions of 25mg/L of Reactive Black treated with 5g/L zero-valent iron obtained in other works [12].

Table 5.2 shows the values that were obtained for the degradation study of Orange II by zero valent iron. The kinetic value decreases as the pH increases, but the order of magnitude is the same (min^{-1}). On the contrary, in our study the kinetic value varies widely with increasing pH at similar temperature, and with a difference of 5 ºC the magnitude order changed.

Table 5. 2. Rate constants for Orange II degradation by Fe.[23]. 0,29 mmol/dm^3 of Orange II at 30^{o}C

pH	(k) (min-1)	R^2
3	0,032	0,973
4	0,018	0,961
5	0,017	0,957
6	0,016	0,886
7	0,014	0,963

Conclusions

Nowadays there are many technologies available for the treatment of wastewater and try to find one suitable technology is very complicated. The best option is to find the whole set of technologies that allows us to treat the effluent in a properly and inexpensive way. One possible option is to use nanoparticles or micro-particles in the tertiary treatment of textile wastewater plants. Probably they should be used in a support inside a column, likewise the active carbon columns. On the other hand, depending on the metal and the production method used, zero-valent nanoparticles may be expensive. However, for this purpose they could be obtained from waste of metallurgical or other industries.

In this work, the degradation of Reactive Black 5 dye by $Mg_{70}Zn_{30}$ metallic glass powders has been studied. However, the results were not satisfactory. Many factors could explain this, such as, the diameter of particles or the composition of the material. The diameter of the particles was similar to other works, and so their surface reaction was more or less the same. In this case, this factor did not explain the huge differences in Mg and Fe zero-valent concerning their capacity to decolourize azo dyes. On the other hand, $Mg_{70}Zn_{30}$ particles were found composed by amorphous phase, crystalline $Mg_{51}Zn_{20}$ phase and MgO. The presence of MgO was a trouble, because this indicates that a fraction of Mg is probably not zero valent. This inhibits the the reaction breaking the N=N bond. For this reason, $Mg_{70}Zn_{30}$ particles were less effective to degrade azo dye. The best option would be tested decolourization experiments with amorphous and semi-amorphous magnesium in order to see the differences.

In the first order kinetics it is normal that at first the reaction proceeds rapidly and then stabilizes, so that an exponential decay is obtained. However, in these decolourization kinetic studies by means of iron, there was a variable period of time depending on the pH and temperature of work that no reaction between the dye and iron occurred. One possible reason is because of other reactions that occurring in a first stage. However, the kinetic value for Reactive Black 5 degradation by Fe in pH = 3 and 20^{o}C was the same order of magnitude (min^{-1}) than other values found in literature.

More work has to be done to improve the procedure method in the laboratory with the available materials. Although a suitable method, using glass tubes and centrifugation, was finally designed and used in this work. The ideal would be to work in a single covered container with constant stirring in a place where you could keep constant temperature in order to minimize errors. In this

study, has been observed that small variations in the amount of metals can cause large differences in dye decolourization. Once developed a good working method, this can be used in the future to found the adequate alloy to decolorize at reasonable speeds around neutral pH and room temperature. It would be also interesting to synthesize a synthetic solution by mixing several dyes in order to imitate the characteristics of real effluents or even work with real effluents. In addition, the final products of the decolourization reaction should be analyzed, in order to know if final products could be toxic or undesired pollutants or not. These analysis would be carried out by HPCL (High-performance liquid chromatography). All this future experiments should allow to discern if this technology is applicable in the treatment of real textile wastewaters.

Bibliography

1. López, C., Moreira Vilar, M. T., Feijoo Costa, G. & Lema, J. M. Tecnologías para el tratamiento de efluentes de industrias textiles. *Afinidad Rev. química teórica y Apl.* **64,** 561–573 (2007).

2. Crespi, M. Tecnologías para la gestión de los efluentes de la industria textil. (2012).

3. Carmen, Z. & Daniela, S. Textile Organic Dyes – Characteristics , Polluting Effects and Separation / Elimination Procedures from Industrial Effluents – A Critical Overview. (2010).

4. Farah Maria Drumond Chequer, G. A. R. de O. E. R. A. F. J. C. C. M. V. B. Z. and D. P. de O. *Eco-Friendly Textile Dyeing and Finishing*. (InTech, 2013). doi:10.5772/3436

5. Ventura-camargo, B. D. C. & Marin-morales, M. A. Azo Dyes : Characterization and Toxicity – A Review. **2,** 85–103 (2013).

6. Zhang, C., Zhu, Z., Zhang, H. & Hu, Z. Rapid reductive degradation of azo dyes by a unique structure of amorphous alloys. *Chinese Sci. Bull.* **56,** 3988–3992 (2011).

7. Riera-Torres, M. & Gutiérrez, M.-C. Colour removal of three reactive dyes by UV light exposure after electrochemical treatment. *Chem. Eng. J.* **156,** 114–120 (2010).

8. Forgacs, E., Cserháti, T. & Oros, G. Removal of synthetic dyes from wastewaters: a review. *Environ. Int.* **30,** 953–71 (2004).

9. Vandevivere, P. C., Bianchi, R. & Verstraete, W. Review: Treatment and reuse of wastewater from the textile wet-processing industry: review of emerging technologies. *J. Chem. Technol. Biotechnol.* **72,** 289–302 (1998).

10. El-Dein, a M., Libra, J. a & Wiesmann, U. Kinetics of decolorization and mineralization of the azo dye reactive black 5 by hydrogen peroxide and UV light. *Water Sci. Technol.* **44,** 295–301 (2001).

11. Patel, R. & Suresh, S. Decolourization of azo dyes using magnesium-palladium system. *J. Hazard. Mater.* **137,** 1729–41 (2006).

12. Pereira, W. S. & Freire, R. S. Azo dye degradation by recycled waste zero-valent iron powder. *J. Braz. Chem. Soc.* **17,** 832–838 (2006).

13. Bahmani, P., Kalantary, R. R., Esrafili, A., Gholami, M. & Jafari, A. J. ENVIRONMENTAL HEALTH Evaluation of Fenton oxidation process coupled

with biological treatment for the removal of reactive black 5 from aqueous solution. 1–9 (2013).

14. Iglesias, O., Fernández de Dios, M. a., Rosales, E., Pazos, M. & Sanromán, M. a. Optimisation of decolourisation and degradation of Reactive Black 5 dye under electro-Fenton process using Fe alginate gel beads. *Environ. Sci. Pollut. Res.* **20,** 2172–83 (2012).

15. Lucas, M. S. & Peres, J. a. Decolorization of the azo dye Reactive Black 5 by Fenton and photo-Fenton oxidation. *Dye. Pigment.* **71,** 236–244 (2006).

16. Lucas, M. S. *et al.* Photocatalytic degradation of Reactive Black 5 with TiO2-coated magnetic nanoparticles. *Catal. Today* **209,** 116–121 (2013).

17. Ucun, H. Equilibrium , thermodynamic and kinetics of reactive black 5 biosorption on loquat (Eriobotrya japonica) seed. **6,** 4113–4124 (2011).

18. Yang, J. F. *et al.* Excellent degradation performance of azo dye by metallic glass/titanium dioxide composite powders. *J. Sol-Gel Sci. Technol.* **67,** 362–367 (2013).

19. Mittal, A., Malviya, A., Kaur, D., Mittal, J. & Kurup, L. Studies on the adsorption kinetics and isotherms for the removal and recovery of Methyl Orange from wastewaters using waste materials. *J. Hazard. Mater.* **148,** 229–40 (2007).

20. Fan, J., Guo, Y., Wang, J. & Fan, M. Rapid decolorization of azo dye methyl orange in aqueous solution by nanoscale zerovalent iron particles. *J. Hazard. Mater.* **166,** 904–10 (2009).

21. Hou, M., Li, F., Liu, X., Wang, X. & Wan, H. The effect of substituent groups on the reductive degradation of azo dyes by zerovalent iron. *J. Hazard. Mater.* **145,** 305–14 (2007).

22. Zhang, W. Nanoscale Iron Particles for Environmental Remediation: An Overview. *J. Nanoparticle Res.* **5,** 323–332 (2003).

23. Mu, Y., Yu, H.-Q., Zhang, S.-J. & Zheng, J.-C. Kinetics of reductive degradation of Orange II in aqueous solution by zero-valent iron. *J. Chem. Technol. Biotechnol.* **79,** 1429–1431 (2004).

24. Cao, J., Wei, L., Huang, Q., Wang, L. & Han, S. Reducing degradation of azo dye by zero-valent iron in aqueous solution. *Chemosphere* **38,** 565–571 (1999).

25. Wang, J.-Q. *et al.* Rapid Degradation of Azo Dye by Fe-Based Metallic Glass Powder. *Adv. Funct. Mater.* **22,** 2567–2570 (2012).

26. Wang, J.-Q. *et al.* Excellent capability in degrading azo dyes by MgZn-based metallic glass powders. *Sci. Rep.* **2,** 418 (2012).

27. Brar, S. K., Verma, M., Tyagi, R. D. & Surampalli, R. Y. Engineered nanoparticles in wastewater and wastewater sludge--evidence and impacts. *Waste Manag.* **30,** 504–20 (2010).

28. Navarro, E. *et al.* Environmental behavior and ecotoxicity of engineered nanoparticles to algae, plants, and fungi. *Ecotoxicology* **17,** 372–86 (2008).

29. Callister, W. D. & Rethwisch, D. G. *Materials science and engineering : an introduction*. (John Wiley, 2007). at <http://cataleg.upc.edu/record=b1294985~S1*cat>

30. Masciangioli, T. & Zhang, W.-X. Peer Reviewed: Environmental Technologies at the Nanoscale. *Environ. Sci. Technol.* **37,** 102A–108A (2003).

31. Weber, E. J. Iron-Mediated Reductive Transformations: Investigation of Reaction Mechanism. *Environ. Sci. Technol.* **30,** 716–719 (1996).

32. Metcalf & Eddy, Tchobanoglous, G., Burton, F. L. & Stensel, H. D. *Wastewater engineering : treatment and reuse*. (McGraw-Hill, 2003). at <http://cataleg.upc.edu/record=b1216627~S1*cat>

33. Salazar, L., Rosell, C. & Salazar, R. Tratamiento de aguas residuales textiles mediante un biorreactor de membrana. (2009).

34. Methyl Orange indicator, Reag. Ph. Eur. | Sigma-Aldrich. at <http://www.sigmaaldrich.com/catalog/product/fluka/32624?lang=es&region=ES>

35. Reactive Black 5 Dye content 55 % | Sigma-Aldrich. at <http://www.sigmaaldrich.com/catalog/product/sial/306452?lang=es&region=ES>

36. Reactive Dyes - Reactive M Dyes, Reactive P Dyes, Reactive ME Dyes. at <http://www.dyespigments.net/reactive-dyes.html>

37. Electrodo de pH 50 14/ 50 14T - Crison Instruments. (2011). at <http://www.crisoninstruments.com/es/laboratorio/electrodos-de-ph/de-cable-fijo-serie-50/electrodos-de-ph-basicos/electrodo-de-ph-50-14-50-14t>

38. Electrodo 50 21/ 50 21T - Crison Instruments. (2011). at <http://www.crisoninstruments.com/es/laboratorio/electrodos-de-ph/de-cable-fijo-serie-50/high-tech-/electrodo-50-21-50-21t>

39. Skoog, D. A. *Química analítica*. (McGraw-Hill, 2001). at <http://cataleg.upc.edu/record=b1204439~S1*cat>

40. UV-2600,UV-2700 UV-VIS Spectrophotometer : SHIMADZU (Shimadzu Corporation). (2013). at <http://www.shimadzu.com/an/spectro/uv/uv2600_2700.html>

41. Chemical Elements.com - An Interactive Periodic Table of the Elements. at <http://www.chemicalelements.com/>

42. Higashi, I., Shiotani, N., Uda, M., Mizoguchi, T. & Katoh, H. The crystal structure of Mg51Zn20. *J. Solid State Chem.* **36,** 225–233 (1981).

Annex

Annex A: Synthesis method

1) Preparing the chamber
   a) Check the melt-spinner state.
   b) Check the exhausting pipe (Orange) is placed correctly with its end out of the lab window
   c) If the chamber is in vacum, fill the chamber with air opening the venting valve V-7.
   d) Put on the gloves.
   e) Put the crucible with the sample inside the induction coil.
   f) Adjust the crucible-wheel distance.
   g) Close chamber doors
2) Primary vacuum
   a) Swich on S-1 and check pressure gauges and pyrometer are connected
   b) Open inert gas bottle, let inert gas fill the pipes opening and closing valves V-4 and V-6
   c) Open red valve V-1 and guillotine valve V-2
   d) Close venting valve V-7
   e) Open V-3 and V-5 valves to ensure vacuum in chamber, crucible and injection containers
   f) Switch on rotary pump
   g) Wait until P < 1 mbar
3) High vacuum
   a) Close red valve V-1
   b) Switch on water pump
   c) Open valve V-8(high vacuum pump cooling)
   d) Switch on high vacuum pump
   e) Wait until P< 10^3 mbar
   f) Close guillotine valve V-2
   g) Close valve V-8 (High vacuum pump cooling)
   h) Switch off high vacuum pump
4) Start cooper wheel rotation
   a) Check the wheel is not in polishing position
   b) Switch on S-2 and S-3

5) Filling chamber and injection containers
   a) Fill chamber opening V-4 up to desired pressure
   b) Close V-4
   c) Close V-3 and V-5
   d) Fill injection containers opening V-6 up to desired pressure
   e) Close V-6
6) Melting and injection
   a) Open V-9(Induction coil cooling)
   b) Switch on S-4
   c) Adjust the desired intensity
   d) Wait until the sample is melted
   e) Open V-5 to inject the melt
7) Stopping the system
   a) Switch off S-3 and S-4
   b) Switch off water pump
   c) Open red valve V-1
   d) Wait until pressure drops enough to ensure exhaustion of chamber gases
   e) Switch off rotary pump
   f) Open venting valve V-7
   g) Open chamber doors and collect ribbons
   h) Clean chamber and wheel using mask while polishing the cooper wheel.
   i) Close gas

Annex B: Solutions preparation

Solutions preparation

HCl 1 M

The HCl was weighted in a beaker. Next the solution was prepared by dissolving 61,63 g HCl in 200 mL of distilled water. The beaker was washed with a little quantities of distilled water. Then the washed water was putted into the volumetric flask. The volumetric flask was filled until 0,5L.

$$\frac{61{,}63\ g\ CD\ HCl}{0{,}5\ L\ DD} x \frac{35\ g\ HCL}{100\ g\ CD\ HCl} x \frac{1\ mol\ HCl}{36{,}47\ g\ HCl} = 1{,}18\ M\ HCl$$

NaOH 0,1M

A solution of NaOH 0,1M was prepared

$$0{,}5\ LDD\ x\frac{0{,}1\ mol\ NaOH}{1\ L\ DD}x\frac{40{,}0\ g\ NaOH}{1\ mol\ NaOH}x\frac{100\ g\ commercial\ product\ NaOH}{99\ g\ NaOH}$$
$$= 2{,}0202\ commercial\ product\ NaOH$$

The NaOH was weighted in a beaker. Next the solution was prepared by dissolving 2,1242 g NaOH in of 200 mL of distilled water. The beaker was washed with a little quantities of distilled water. Then the washed water was putted into the volumetric flask. The volumetric flask was filled until 0,5L.

$$\frac{2{,}1242\ g\ commercial\ product\ NaOH}{0{,}5\ L\ DD}x\frac{99\ g\ \ Na0H}{100\ g\ commercial\ product\ NaOH}x\frac{1\ mol\ NaOH}{40{,}0\ g\ NaOH}$$
$$= 0{,}105\ M\ NaOH$$

NaOH 1M

$$0{,}5\ LDD\ x\frac{1\ mol\ NaOH}{1\ L\ DD}x\frac{40{,}0\ g\ NaOH}{1\ mol\ NaOH}x\frac{100\ g\ commercial\ product\ NaOH}{99\ g\ NaOH}$$
$$= 20{,}20\ commercial\ product\ NaOH$$

In this case the procedure was the same than before. But the quantity of NaOH weighted was 19,8285 g.

$$\frac{19{,}8285\ gcommercial\ product\ NaOH}{0{,}5\ L\ DD}x\frac{99\ g\ \ Na0H}{100\ g\ commercial\ product\ NaOH}x\frac{1\ mol\ NaOH}{40{,}0\ g\ NaOH}$$
$$= 0{,}9815\ M\ NaOH$$

Reactive Black 5 acid solution (pH≈3)

Acetic acid commercial	
Assay (%)	99,7
Density (20/4)(kg/L)	1,048- 1,050
M (g/mol)	60,05

Table 1: Characteristics of acetic acid.

The purpose was to prepare a solution 0,087 M of acetic acid.

$$1LDD\ x\frac{0{,}087\ mol\ acetic\ ac}{1\ L\ DD}x\frac{60{,}05\ g\ acetic\ ac.}{1\ mol\ acetic\ ac.}x\frac{100\ g\ DC}{99{,}7\ g\ acetic\ ac.}x\frac{1\ L\ DC}{1050\ g\ DC}$$
$$= 4{,}99x10^{-3}\ L\ DC$$

Firstly, the acid acetic was weighted in a beaker. A solution of acetic acid 87 mM was prepared by dissolving 5,5204 g acid acetic around of 200 mL of distilled water. This solution was stirred and it was transferred to a 1L volumetric flask. The beaker was washed three times with approximately 100 mL of distilled water. Then this water was putted into volumetric flask. After the volumetric flask was filled to 1L and it was mixed. Finally, the pH were measured by pHmeter.

$$\frac{5{,}5204\ g\ DC}{1\ L\ DD}x\frac{99{,}7\ g\ acetic\ acid}{100\ g\ DC}x\frac{1\ mol\ acetic\ acid}{60{,}05\ g\ acetic\ acid}=0{,}0917\ M\ acetic\ acid$$

The concetration was obtained 92 mM.

Reactive Black 5 commercial	
Dye content (%)	55
M(g/mol)	991,82

Table 2: Characteristics of Reactive Black 5.

$$1L\ DS\ x\frac{0{,}1107x10^{-3}mol\ dye}{1\ L\ DS}x\frac{991{,}82\ g\ dye}{1\ mol\ dye}x\frac{100\ g\ powder}{55\ g\ dye}=0{,}1996\ g\ powder$$

Afterward, the powder solution was prepared by dissolving 204,3 mg of powder in 250 mL of the acid acetic solution had prepared before. Next, all the acid acetic solution was mixed with the powder. All the solution was mixed and it was kept in a dark bottle.

$$\frac{0{,}2043\ g\ powder}{1\ L\ DD}x\frac{55\ g\ dye}{100\ g\ powder}x\frac{1\ mol\ dye}{991{,}82\ g\ dye}=1{,}13\ x\ 10^{-4}\ M\ dye\ solution$$

Reactive Black 5 solution(pH≈4)

In this case the dye solution was prepared by dissolving 199,9 mg of powder in 1L of distilled water. One drop of commercial acetic acid was added to obtain pH≈4. The pH was checked by pHmeter.

$$\frac{0{,}1999\ g\ powder}{1\ L\ DD} x \frac{55\ g\ dye}{100\ g\ powder} x \frac{1\ mol\ dye}{991{,}82\ g\ dye} = 1{,}11\ x\ 10^{-4}\ M\ dye$$

Reactive Black 5 neutral solution(pH≈6.5)

In this case the dye solution was prepared by dissolving 201,0 mg of powder in 1L of distilled water. The same way at the step before.

$$\frac{0{,}201\ g\ powder}{1\ L\ DD} x \frac{55\ g\ dye}{100\ g\ powder} x \frac{1\ mol\ dye}{991{,}82\ g\ dye} = 1{,}11\ x\ 10^{-4}\ M\ dye$$

Annex C: Results tables

Table 1. Percentage of atomic composition was analized by SEM and normalized percentage of atomic composition.

Id.	%C	%O	%Mg	%Si	%Zn	%total	% at normalized sample	% at normalized Mg	% at normalized Zn
SAP1R B1SP1	0,00	0,00	68,20	0,81	30,99	100,00	99,19	68,76	31,24
SAP1R B1SP2	0,00	0,00	69,30	0,72	29,98	100,00	99,28	69,80	30,20
SAP1R B2SP1	6,00	0,00	64,20	0,60	29,21	100,01	93,40	68,74	31,27
SAP1R B2SP2	6,73	0,00	65,72	0,77	26,79	100,01	92,50	71,05	28,96
SAP1R B3SP1	4,24	0,00	66,37	0,63	28,75	99,99	95,13	69,77	30,22
SAP1R B3SP2	6,81	0,00	63,15	0,65	29,39	100,00	92,54	68,24	31,76
SAP1R B4SP1	7,89	0,00	63,20	0,60	28,32	100,01	91,51	69,06	30,95
SAP1R B4SP2	4,14	0,00	65,86	0,75	29,25	100,00	95,11	69,25	30,75
SAP1R B4SP3	5,55	0,00	64,52	0,64	29,30	100,01	93,81	68,78	31,23
SAP1R B5SP1	5,89	0,00	64,35	0,76	29,00	100,00	93,35	68,93	31,07
SAP1R B5SP2	7,70	0,00	62,49	0,68	29,13	100,00	91,62	68,21	31,79
SAP1R B6SP1	8,34	0,00	62,50	0,70	28,46	100,00	90,96	68,71	31,29
SAP1R B6SP2	10,64	0,00	60,09	0,70	28,58	100,01	88,66	67,77	32,24

SAP1R B7SP1	11,17	0,00	60,69	0,78	27,36	100,00	88,05	68,93	31,07
SAP1R B7SP2	10,09	0,00	59,73	0,56	29,62	100,00	89,35	66,85	33,15
SAP2R B1SP1	16,10	1,31	54,69	0,39	27,52	100,01	82,20	66,53	33,48
SAP2R B1SP2	9,20	3,24	59,52	0,53	27,52	100,01	87,03	68,39	31,62
SAP2R B2SP1	7,38	4,49	53,31	0,42	34,40	100,00	87,71	60,78	39,22
SAP2R B2SP2	8,27	3,67	52,29		35,77	100,00	88,06	59,38	40,62
SAP2R B3SP1	8,04	0,00	65,44	0,72	25,80	100,00	91,24	71,72	28,28
SAP2R B3SP2	15,47	0,00	59,05	0,49	25,00	100,01	84,04	70,26	29,75
SAP2R B4SP1	41,31	0,00	40,53		18,16	100,00	58,69	69,06	30,94
SAP2R B4SP2	0,00	0,00	72,05	0,69	27,26	100,00	99,31	72,55	27,45
SAP2R B4SP3	0,00	0,00	72,09		27,91	100,00	100,00	72,09	27,91
SAP2R B5SP1	4,49	0,00	67,38	0,56	27,56	99,99	94,95	70,96	29,03
SAP2R B5SP2	12,94	0,00	61,18	0,52	25,36	100,00	86,54	70,70	29,30
SAP3R B1SP1	6,47	1,16	64,56		27,81	100,00	92,37	69,89	30,11
SAP3R B1SP2	6,95	1,33	64,99		26,72	99,99	91,72	70,86	29,13
SAP3R B2SP1			70,94		29,06	100,00	100,00	70,94	29,06
SAP3R B2SP2			69,72		30,28	100,00	100,00	69,72	30,28
SAP3R B2SP3			70,90		29,10	100,00	100,00	70,90	29,10
Mean	8,28	0,54	63,19	0,64	28,37	100,00	91,56	68,95	31,05

Table 2. Diameter of Fe particles

Particle number	Size H (pixels)	Size V (pixels)	H diameter (µm)	V diameter (µm)	Average diameter (µm)
1	50	48	11,91	11,4336	11,6718
2	24	26	5,7168	6,1932	5,955
3	39	23	9,2898	5,4786	7,3842
4	32	29	7,6224	6,9078	7,2651
5	69	66	16,4358	15,7212	16,0785

6	30	29	7,146	6,9078	7,0269
7	33	43	7,8606	10,2426	9,0516
8	76	40	18,1032	9,528	13,8156
9	21	21	5,0022	5,0022	5,0022
10	78	60	18,5796	14,292	16,4358
11	39	29	9,2898	6,9078	8,0988
12	43	18	10,2426	4,2876	7,2651
13	19	21	4,5258	5,0022	4,764
14	24	23	5,7168	5,4786	5,5977
15	23	26	5,4786	6,1932	5,8359
16	63	63	15,0066	15,0066	15,0066
17	12	20	2,8584	4,764	3,8112
18	24	24	5,7168	5,7168	5,7168
19	44	46	10,4808	10,9572	10,719
20	22	29	5,2404	6,9078	6,0741
21	35	49	8,337	11,6718	10,0044
22	79	57	18,8178	13,5774	16,1976
23	38	31	9,0516	7,3842	8,2179
24	53	68	12,6246	16,1976	14,4111
25	44	31	10,4808	7,3842	8,9325
26	21	19	5,0022	4,5258	4,764
27	77	45	18,3414	10,719	14,5302
28	35	26	8,337	6,1932	7,2651
29	30	23	7,146	5,4786	6,3123
30	37	30	8,8134	7,146	7,9797
31	22	17	5,2404	4,0494	4,6449
32	57	49	13,5774	11,6718	12,6246
33	59	27	14,0538	6,4314	10,2426
34	37	42	8,8134	10,0044	9,4089
35	32	46	7,6224	10,9572	9,2898
36	33	15	7,8606	3,573	5,7168
37	17	46	4,0494	10,9572	7,5033
38	40	24	9,528	5,7168	7,6224
39	24	41	5,7168	9,7662	7,7415
40	31	46	7,3842	10,9572	9,1707
41	33	19	7,8606	4,5258	6,1932
42	20	32	4,764	7,6224	6,1932
43	22	24	5,2404	5,7168	5,4786
44	15	29	3,573	6,9078	5,2404
45	19	26	4,5258	6,1932	5,3595
46	18	18	4,2876	4,2876	4,2876
47	20	18	4,764	4,2876	4,5258
48	21	18	5,0022	4,2876	4,6449

49	18	48	4,2876	11,4336	7,8606
50	24	14	5,7168	3,3348	4,5258

Table 3. Diameter of MgZn particles

Particle number	Size H (pixels)	Size V (pixels)	H diameter (µm)	V diameter (µm)	Average diameter (µm)
1	141	70	33,5862	16,674	25,1301
2	26	27	6,1932	6,4314	6,3123
3	56	30	13,3392	7,146	10,2426
4	20	24	4,764	5,7168	5,2404
5	30	31	7,146	7,3842	7,2651
6	25	23	5,955	5,4786	5,7168
7	27	20	6,4314	4,764	5,5977
8	31	33	7,3842	7,8606	7,6224
9	21	20	5,0022	4,764	4,8831
10	49	45	11,6718	10,719	11,1954
11	50	39	11,91	9,2898	10,5999
12	111	72	26,4402	17,1504	21,7953
13	28	18	6,6696	4,2876	5,4786
14	17	17	4,0494	4,0494	4,0494
15	43	19	10,2426	4,5258	7,3842
16	39	31	9,2898	7,3842	8,337
17	37	32	8,8134	7,6224	8,2179
18	13	33	3,0966	7,8606	5,4786
19	19	15	4,5258	3,573	4,0494
20	114	51	27,1548	12,1482	19,6515
21	62	52	14,7684	12,3864	13,5774
22	184	101	43,8288	24,0582	33,9435
23	26	27	6,1932	6,4314	6,3123
24	49	39	11,6718	9,2898	10,4808
25	29	31	6,9078	7,3842	7,146
26	26	32	6,1932	7,6224	6,9078
27	112	86	26,6784	20,4852	23,5818
28	38	45	9,0516	10,719	9,8853
29	33	52	7,8606	12,3864	10,1235
30	31	32	7,3842	7,6224	7,5033
31	46	23	10,9572	5,4786	8,2179
32	20	25	4,764	5,955	5,3595
33	37	20	8,8134	4,764	6,7887
34	41	32	9,7662	7,6224	8,6943
35	29	30	6,9078	7,146	7,0269

36	18	22	4,2876	5,2404	4,764
37	32	37	7,6224	8,8134	8,2179
38	29	24	6,9078	5,7168	6,3123
39	13	43	3,0966	10,2426	6,6696
40	42	54	10,0044	12,8628	11,4336
41	62	54	14,7684	12,8628	13,8156
42	49	57	11,6718	13,5774	12,6246
43	29	34	6,9078	8,0988	7,5033
44	16	48	3,8112	11,4336	7,6224
45	28	21	6,6696	5,0022	5,8359
46	20	35	4,764	8,337	6,5505
47	45	64	10,719	15,2448	12,9819
48	44	23	10,4808	5,4786	7,9797
49	14	17	3,3348	4,0494	3,6921
50	64	26	15,2448	6,1932	10,719